

Geometry of quantum states and chaos-integrability transition

Ankit Gill,^{1,*} Keun-Young Kim,^{2,3,†} Kunal Pal,^{4,‡} and Kuntal Pal^{2,§}

¹*Department of Physics, Indian Institute of Technology, Kanpur 208016, India*

²*Department of Physics and Photon Science, Gwangju Institute of Science and Technology,
123 Cheomdan-gwagiro, Gwangju 61005, Republic of Korea*

³*Research Center for Photon Science Technology, Gwangju Institute of
Science and Technology, 123 Cheomdan-gwagiro, Gwangju 61005, Korea*

⁴*Asia Pacific Center for Theoretical Physics, Pohang 37673, Republic of Korea*

We consider the geometry of quantum states associated with classes of random matrix Hamiltonians, in particular ensembles that show integrability to chaotic transition in terms of the nearest neighbour energy level spacing distribution. In the case that the total Hamiltonian contains a single parameter, the distance between two states is captured by the fidelity susceptibility, whereas, when the total Hamiltonian contains multiple parameters, this distance is given by the quantum metric tensor. Since the fidelity susceptibility is closely related to the two-point correlation function, we first calculate the relevant correlation functions of a random matrix belonging to the Gaussian unitary ensemble in terms of the spectral form factor of the total Hamiltonian, show how to obtain the fidelity susceptibility from this correlation function, and explain the role played by energy level correlation. Next, by performing suitable coordinate transformations, we solve the geodesic equations corresponding to the quantum metric tensor obtained from an integrability-breaking random matrix Hamiltonian and obtain the geodesic distance between two points on the parameter manifold to show that any point far away from the integrable phase can be reached by a finite value of this distance. Finally, we obtain and discuss different properties of the fidelity susceptibility associated with Hamiltonians belonging to another random matrix ensemble which shows integrability to chaos transition, namely the Gaussian β -ensembles with general values of the Dyson index β , and show that the fidelity susceptibility shares generic features with the first class of Hamiltonians.

I. INTRODUCTION

Geometric approaches have become increasingly valuable in quantum many-body physics, offering deep insights into the structure of quantum states beyond conventional symmetry-based classifications. The geometry of pure quantum states is naturally described on the complex projective Hilbert space, where the Hermitian inner product of the ambient Hilbert space induces both a Riemannian and a symplectic structure [1, 2]. Specifically, the real part of the quantum geometric tensor defines a real, symmetric metric that governs the infinitesimal distance between nearby states (the quantum or Fubini-Study metric), while its imaginary part gives rise to the Berry curvature, a real-valued antisymmetric two-form that encodes the underlying symplectic structure. These structures together endow the projective Hilbert space with the geometry of a Kähler manifold, capturing both the metric and topology [3–5].

The quantum geometric tensor (QGT), which is a pullback of the Fubini-Study tensor on the parameter manifold, was introduced by Provost and Vallee and provides a unified framework for characterising both the geometric and topological aspects of quantum states in parameter space [6]. Defined on the manifold of quantum states, the QGT decomposes into two components: the quantum metric tensor (QMT), which quantifies the distance between infinitesimally close states, and

the Berry curvature, which governs geometric phases under adiabatic evolution [7, 8]. By capturing how quantum states change under smooth variations of parameters, geometry provides a natural language for exploring quantum phase transitions and topological phenomena.

In the context of quantum phase transitions, the QMT has emerged as a sensitive probe of criticality, capturing singular behaviour near critical points even when conventional order parameters are absent [9–18]. Meanwhile, the Berry curvature part of the QGT encodes the system’s response to adiabatic perturbations and underlies a variety of topological invariants, such as Chern numbers, which, in the linear response theory formalism, can be attributed to the QGT contributions to the generalized susceptibilities and dynamical response functions, linking geometric properties of quantum states to measurable quantities [19–21]. In this paper, we use the geometry of quantum states of a random matrix Hamiltonian belonging to an ensemble of matrices to characterise the transition from integrability to chaos in these ensembles.

One of the most useful ways of understanding dynamical and spectral properties of quantum systems is to use random matrix theory to model its spectral statistics. The wide range of usages of random matrix theory in physics is due to the fact that it has many powerful mathematical tools that one can employ to study statistical properties of physical quantities associated with extremely complex quantum systems. The random matrices can describe universal properties that do not depend on the details of a given system, but rather are determined by a set of global symmetries that are commonly shared by all systems in a given symmetry class.

The classical Gaussian random matrix ensembles studied by Wigner and Dyson [22] have been used to understand the characteristic properties, namely the level repulsion and rigid-

* ankitgill20@iitk.ac.in

† fortoc@gist.ac.kr

‡ kunal.pal@apctp.org

§ kuntalpal@gist.ac.kr

ity of the energy spectrum of quantum systems having classically chaotic counterparts [23, 24]. On the other hand, in integrable systems, the energy eigenvalues are uncorrelated random numbers; hence, the distribution of the nearest neighbour level energy spacing follows the Poisson statistics.

However, in many physical situations, quantum systems can consist of parts of different symmetries, or can have classically chaotic and integrable counterparts. If a parameter exists in such systems, such that changing it causes the system to make a transition from different symmetry classes, then these transitions would be reflected in the symmetry class of the corresponding random matrix. Therefore, in those cases, the quantum systems can also follow other level spacing statistics, which are intermediate between the Wigner-Dyson statistics of classical Gaussian ensembles and Poisson statistics of integrable systems [25–30].

The classical random matrix ensembles are defined with two conditions: 1. the matrix elements are sampled from independent distributions, and 2. the probability distribution ($P(H)$) of obtaining a particular instance of the matrix H is invariant under a symmetry transformation. E.g., for the Gaussian unitary ensemble (GUE), the probability distribution is invariant under unitary transformation of H [31, 32]. Therefore, in order to capture the spectral statistics intermediate between the Wigner-Dyson and Poisson, one presumably needs to consider more general random matrix ensembles, where one of the above two constraints is relaxed.

The Rosenzweig-Porter (RP) model, which was originally introduced to explain the properties of the spectrum of atoms, is one such random matrix ensemble where the assumption of invariance under a symmetry transformation is relaxed compared to the classical Gaussian ensembles by introducing a parameter that spoils the usual relation between the variance of the diagonal and off-diagonal elements [33–37]. By tuning this parameter suitably, one can get the Poisson and Wigner-Dyson statistics of the energy level spacing distribution as two limits of the RP model. In its most commonly used form, the RP model consists of a diagonal matrix whose elements are sampled from independent and identically distributed random variables (usually from Gaussian distributions with a zero mean), and a random matrix (usually drawn from one of the classical Gaussian ensembles) is added to the diagonal matrix as a perturbation term.¹ This form for the Hamiltonian of the RP model makes it particularly suitable for studying the geometry of quantum states, as the level spacing statistics makes a transition from Poissonian to Wigner-Dyson statistics.

Another class of random matrix ensembles that show the transition from integrability and chaos in terms of the level spacing distribution is the so-called Gaussian β -ensembles, where the Dyson index β can take any real positive value. A convenient sparse tridiagonal matrix form of these ensembles was constructed in [40]. This class of ensembles also breaks the rotational invariance of the classical Gaussian ensembles,

and shows integrability to chaos transition when the Dyson index is varied [41]. An important difference between these ensembles and the classical Gaussian β -ensemble lies in the nature of eigenstates. Namely, due to the rotational invariance of the classical Gaussian ensembles, the eigenstates of a Hamiltonian sampled from these are uniformly distributed on the surface of a multidimensional sphere and have mutually independent components in terms of a complete basis, whereas, for a Hamiltonian sampled from the Gaussian β -ensembles, roughly, if the first row of the eigenvector matrix is specified, one can obtain the full expression for the eigenstates from the eigenvalues, and the elements of the tridiagonal form of the Hamiltonian [40].

In this paper, we use both of these generalised random matrix ensembles to analyse the geometry of quantum states of Hamiltonians drawn from these. In the first part of the paper, after briefly reviewing the definitions of the QGT, QMT and ensemble-averaged QMT in section II, we study the geometric quantities associated with the ensemble-averaged QMT (originally derived in [42]) obtained from a GUE Hamiltonian and an integrability-breaking Hamiltonian that is a generalisation of the RP model. Specifically, in section III and V we find out suitable coordinate transformations which make the QMTs derived in [42] much simpler to work with. In terms of these coordinates, one can then solve the geodesic equations associated with the metric tensor and obtain the geodesic distance between two points on the space of parameters, which helps to understand the chaos-to-integrability transition in terms of this geometric quantity. In particular, we show that any point far away from the integrable point can be reached by a finite geodesic distance.

It is well-known that the fidelity susceptibility (FS), as well as the QMT, are closely related to the real and imaginary time correlation functions of physical operators for any generic Hamiltonian [10, 43–45]. To understand this connection more clearly in the context of random matrices, in section IV we compute a class of correlation functions involving a GUE matrix analytically and show how to get back the components of the metric tensor from this correlation function. As we show, these classes of correlation functions are directly related to the spectral form factor (SFF) [32, 46]. This, on the one hand, makes the physical implication of the FS clearer, while on the other hand, it also relates the geometry of quantum states of these random matrix ensembles with one of the most commonly used quantifiers of the chaotic nature of the energy spectrum, namely the SFF.

In the second part, we obtain the geometry of eigenstates belonging to the tridiagonal Gaussian β -ensembles, which also show integrability to chaos transition with varying Dyson index. Assuming the total Hamiltonian is a sum of two terms, a 2×2 matrix belonging to this ensemble, which is added to a diagonal Hamiltonian, we obtain an analytical expression for the FS for any generic value of the Dyson index, and study its behaviour with respect to the change of the relevant parameters (section VI). We show that the FS shares generic features with those of the generalised RP model. Furthermore, to complement the analysis of the tridiagonal ensembles which break the rotational invariance of the classical Gaussian ensembles,

¹ There appeared other generalisations of this particular form of the RP model in the literature. See, e.g., [34, 38, 39].

an invariant 2×2 random matrix ensemble with an effective Dyson index is also analysed, and we show that the FS still captures the essential signature of the chaos-to-integrability transition (see section VII).

This paper also contains several appendices where we provide some details that are left out of the main text. Specifically, in Appendix B we have outlined the steps of the derivation of the components of the QGT for the GUE Hamiltonian, and in Appendix D we have provided an alternative derivation of the correlation function computed in section IV, which is directly related to the components of the metric tensor. Finally, in Appendix E, the expression for the FS of a specific random matrix ensemble, whose eigenvalues are drawn from a Gaussian β -ensemble with generic β and has Haar random eigenstates, is obtained, and its properties are discussed.

II. FIDELITY SUSCEPTIBILITY AND QUANTUM METRIC TENSOR FOR RANDOM MATRIX ENSEMBLES

In this section, we first review the definition of the fidelity susceptibility (FS) associated with a change in one of the parameters of the Hamiltonian of a quantum system, and then discuss its generalisation when more than one of the Hamiltonian parameters are changed - a situation where a metric structure naturally appears in the space of eigenstates.

To begin with, we consider the simplest scenario, i.e., a system whose total Hamiltonian is given by²

$$H(r) = H_0 + r \mathcal{H}, \quad (1)$$

where r is a positive parameter. Now consider the change in the fidelity of the n th eigenstate $|n(r)\rangle$ of the Hamiltonian H in (1), i.e., change in $\mathcal{F}(r, dr) = |\langle n(r)|n(r + \delta r)\rangle|^2$.³ Expanding the fidelity for small values of δr , and using the normalisation of the states $|n(r)\rangle$ one has in the limit $\delta r \rightarrow 0$, the following expansion

$$\mathcal{F}(r, \delta r \rightarrow 0) \simeq 1 - (\delta r)^2 g_{rr}^n(r). \quad (2)$$

Here $g_{rr}^n(r)$ is FS of the n -th eigenstates, and a straightforward

calculation shows that its expression can be written as⁴ [9]

$$g_{rr}^n(r) = \langle \partial_r n(r) | \partial_r n(r) \rangle - \langle \partial_r n(r) | n(r) \rangle \langle n(r) | \partial_r n(r) \rangle \\ = \sum_{j(\neq n)} \frac{\mathcal{H}_{nj} \mathcal{H}_{jn}}{(E_j(r) - E_n(r))^2}. \quad (3)$$

Here $\mathcal{H}_{nj} = \langle n | \mathcal{H} | j \rangle$ denotes the matrix elements of \mathcal{H} in the basis of $|n\rangle$, the eigenstate of H . Note that this quantity is invariant under an overall constant scaling transformation of the Hamiltonian $H(r)$.

Summing over the expressions for the FS $g_{rr}^n(r)$ for all the energy eigenstates, we define an averaged FS as follows

$$g_{rr}(r) = \frac{1}{N} \sum_{n=1}^N g_{rr}^n(r) = \frac{1}{N} \sum_{j \neq n} \frac{\mathcal{H}_{nj} \mathcal{H}_{jn}}{(E_j(r) - E_n(r))^2}, \quad (4)$$

where N denotes the dimension of the Hilbert space of the Hamiltonian H . Note that this quantity may not have any interpretation as the fidelity susceptibility of a single generic pure state which is a linear combination of the energy eigenstates.

Now assume that H_0 and \mathcal{H} are independent random matrices of rank N , and the probability distribution for the total Hamiltonian (H) is given by

$$P(H) = \frac{1}{\mathcal{Z}_{\beta, N}} \exp \left[-\frac{\beta N}{4} \text{Tr} \left(V_0(H_0) + \mathcal{V}(\mathcal{H}) \right) \right], \quad (5)$$

where $\mathcal{Z}_{\beta, N}$ is a normalisation constant whose form also depends on the expressions for the potentials $V_0(H_0)$ and $\mathcal{V}(\mathcal{H})$, and β is the Dyson index of the ensemble. For later purposes, here we note that the well-known expression for the joint probability distribution (JPD) of the eigenvalues (E_i) of a rationally invariant $N \times N$ random matrix ensemble with a confining potential $V(H) = \sum_n \alpha^n \text{Tr}(H^n)$ is given by [31, 32]

$$P(E_1, \dots, E_N) = \frac{1}{Z(\beta, N)} e^{-\frac{\beta N}{4} \sum_n \alpha_n \sum_{i=1}^N E_i^n} \prod_{j < k} |E_j - E_k|^\beta, \quad (6)$$

where $Z(\beta, N)$ is a normalization constant, and α_n s are a set of real constants. For the case of the total Hamiltonian is given by the one in (1), since the random matrices H_0 and \mathcal{H} are also free in the large N limit ($N \rightarrow \infty$) [47, 48], the probability distribution factorises, and when we perform an average of the FS over the ensembles, the ensemble-averaged FS can be written as⁵

$$\bar{g}_{rr}(r) = \mathbb{E}(g_{rr}(r)) = \int dH(\mathbf{r}) P(H(r)) g_{rr}(r) = \frac{1}{N} \sum_{j \neq n} \int \frac{\mathcal{H}_{nj} \mathcal{H}_{jn}}{(E_j(r) - E_n(r))^2} P(H_0) P(\mathcal{H}) dH_0 d\mathcal{H}. \quad (7)$$

² We assume that the Hamiltonian H has no degeneracy in the spectrum.

³ Some authors define the fidelity as the absolute value of the overlap between the eigenstate at a parameter value r , and at $r + \delta r$.

⁴ In this paper we use the convention that $\sum_{j(\neq n)}$ denotes sum over all j , except n , and no sum over the index n . On the other hand, $\sum_{j \neq n}$ denotes the sum over both j and n , excluding the cases when $j = n$.

⁵ Since, in this paper we always consider random matrix Hamiltonians, all the relevant quantities are obtained with an average over the ensemble. Hence, we often omit explicitly referring to the quantifier 'ensemble-averaged'.

Here $P(H_0)$ and $P(\mathcal{H})$ are the distributions for the independent random matrices H_0 and \mathcal{H} , respectively. In this paper, we mostly consider Gaussian random matrices, for which the potential function is $V(H) = H^2$.

A. Connection with correlation functions

The FS can be related to the unequal time correlation function of physical operators. To see this explicitly, first consider the following trick to relate the Kallen-Lehmann representation of an operator to its unequal time correlation function,

$$\frac{1}{(E_j(r) - E_n(r))^2} = \int_{-\infty}^{\infty} \frac{d\omega}{\omega^2} \int_{-\infty}^{\infty} \frac{dt}{2\pi} e^{-i(E_j(r) - E_n(r) - \omega)t} . \quad (8)$$

Using this relation, we can write the FS in eq. (3) as [43, 44]

$$g_{rr}^n(r) = \frac{1}{2\pi} \int_{-\infty}^{\infty} \frac{d\omega}{\omega^2} \mathcal{S}^n(\omega) , \quad (9)$$

where

$$\mathcal{S}^n(\omega) = \int_{-\infty}^{\infty} dt e^{i\omega t} \left(\langle n | \mathcal{H}(t) \mathcal{H} | n \rangle - |\langle n | \mathcal{H} | n \rangle|^2 \right) , \quad (10)$$

and $\mathcal{H}(t) = e^{iHt} \mathcal{H} e^{-iHt}$.

Now summing over all the eigenstates $|n\rangle$ and averaging over the random matrix ensemble, in the case $H(r)$ belongs to one, we have the following relation

$$\bar{g}_{rr}(r) = \frac{1}{2\pi} \int_{-\infty}^{\infty} \frac{d\omega}{\omega^2} \mathcal{S}(\omega) , \quad (11)$$

where we have defined the spectral function

$$\mathcal{S}(\omega) = \int_{-\infty}^{\infty} dt e^{i\omega t} \left(\langle \mathcal{H}(t) \mathcal{H} \rangle - \frac{1}{N} \mathbb{E} \sum_n |\langle n | \mathcal{H} | n \rangle|^2 \right) , \quad (12)$$

with the symbol \mathbb{E} denoting an ensemble average over the probability distribution of the Hamiltonian $H(r)$, and we have used the following notation to denote the map which combines the trace and the ensemble average,

$$\langle O \rangle = \varphi_N(O) = \frac{1}{N} \mathbb{E} \left(\text{Tr}(O) \right) . \quad (13)$$

We continue to use this notation in the following. This map can be thought of as the inner product with respect to the infinite temperature thermofield double state.

The relation in (11), an alternative way of obtaining the FS would be to calculate the following ensemble-averaged two-point correlation function of the operator \mathcal{H} ,

$$G(t) = \langle \mathcal{H}(t) \mathcal{H} \rangle = \varphi_N(\mathcal{H}(t) \mathcal{H}) = \frac{1}{N} \mathbb{E} \left(\text{Tr}(\mathcal{H}(t) \mathcal{H}) \right) , \quad (14)$$

and use it in the eq. (11) along with (12). In section IV, we obtain an analytical expression for this correlation function when $H(r)$ belongs to a GUE, and discuss its connection with

the SFF, and subsequently show how to obtain the FS from this correlation function.

Note that we can rewrite the expression for the spectral function $\mathcal{S}(\omega)$ as

$$\mathcal{S}(\omega) = \frac{2\pi}{N} \mathbb{E} \sum_{n \neq j} |\mathcal{H}_{nj}|^2 \delta(E_j - E_n - \omega) . \quad (15)$$

Considering the moments of this function,

$$m_k(r) = \mathbb{E} \int d\omega \omega^k \mathcal{S}(\omega) = \frac{2\pi}{N} \mathbb{E} \sum_{n \neq j} |\mathcal{H}_{nj}|^2 (E_j(r) - E_n(r))^k , \quad (16)$$

we see that these have direct physical meanings. For example, $m_{-2}(r)$ is nothing but the averaged FS (with a proportionality constant 2π). We also note that the function $\mathcal{S}(\omega)$ is the frequency space expression of the connected correlation function, and is related to the dynamical susceptibility of the system through the Kubo linear response formula.

B. Quantum metric tensor

The expressions for the FS discussed so far can be generalised when the system Hamiltonian depends on more than one parameter r^1, \dots, r^k , which we collectively denote as \mathbf{r} . In that case, it is convenient to define the following ‘line element’, which incorporates changes in one or more of the parameters,

$$ds^2 \equiv 1 - |\langle n(\mathbf{r}) | n(\mathbf{r} + d\mathbf{r}) \rangle|^2 \equiv g_{ab}^n(\mathbf{r}) d\mathbf{r}^a d\mathbf{r}^b + O(|d\mathbf{r}|^3) , \quad (17)$$

where the expression for the QMT for the n -th eigenstate can be written as

$$g_{ab}^n(\mathbf{r}) = \sum_{m(\neq n)} \frac{\langle n(\mathbf{r}) | \partial_a H(\mathbf{r}) | m(\mathbf{r}) \rangle \langle m(\mathbf{r}) | \partial_b H(\mathbf{r}) | n(\mathbf{r}) \rangle}{(E_m - E_n)^2} , \quad (18)$$

where we have denoted $\partial_a = \partial_{r^a}$. For a Hermitian Hamiltonian, as expected, this quantity is real and symmetric in the indices a and b .

A related quantity studied in [42] for Hamiltonians belonging to random matrix ensembles is called the averaged QMT, and is defined as⁶

$$g_{ab}(\mathbf{r}) = \frac{1}{N} \sum_{n=1}^N g_{ab}^n(\mathbf{r}) . \quad (19)$$

When the Hamiltonian H belongs to some random matrix ensemble, we perform an average of the QMT components over the ensemble, and define an ensemble-averaged QMT as

$$\bar{g}_{ab}(\mathbf{r}) = \mathbb{E}(g_{ab}(\mathbf{r})) = \int dH(\mathbf{r}) P(H(\mathbf{r})) g_{ab}(\mathbf{r}) , \quad (20)$$

⁶ In Appendix. A we have provided the generic expression for the QGT of a state which is a superposition of the eigenstates of the system Hamiltonian.

where $P(H)$ denotes the probability weight associated with the ensemble from which the total Hamiltonian is drawn.

Before moving on, a comment on the difference between the quantity defined in (3) and a similar quantity studied in the context of random matrices in [49] is in order. In defining the quantity (3) we have assume H to be total Hamiltonian and consider applying a perturbation term of the form $\delta r \mathcal{H}$ which give rise to the FS in (3) and the expectation value of \mathcal{H} are with respect to the eigenstates $|n\rangle$ of the total Hamiltonian. On the other hand, one can consider a scenario where H_0 is the initial Hamiltonian and the term $r\mathcal{H}$ acts as a perturbation. In that case, one can derive an identical-looking expression for the associated FS where the matrix elements of \mathcal{H} are with respect to $|n_0\rangle$ the eigenstates of H_0 , and in the denominator the energy difference term would be $(E_n^0 - E_j^0)^2$.

III. GEOMETRIC PROPERTIES OF QMT OF THE GAUSSIAN UNITARY RANDOM MATRIX ENSEMBLES

A. Components of the quantum metric tensor

We first consider the scenario where the total Hamiltonian belongs to one of the classical Gaussian ensembles, which we take to be GUE here. Specifically, we parametrise the total Hamiltonian of the system such that it can be written as [50, 51]

$$H(r, \phi) = H_0 + r \cos \phi \mathcal{H}_1 + r \sin \phi \mathcal{H}_2, \quad (21)$$

where \mathcal{H}_i , $i = 0, 1, 2$ are three $N \times N$ matrices drawn independently from the GUE with zero mean and variance σ^2 . These fix the variance of the total Hamiltonian (H) to be $\sigma^2(r^2 + 1)$. In this paper, unless stated otherwise, we shall take $\sigma^2 = 1/N$. Furthermore, $0 \leq r < \infty$ and $0 \leq \phi \leq 2\pi$ are two parameters, which are coordinates in terms of which the components of the QMT will be written.

For this Hamiltonian, the components of the ensemble-averaged QMT in eq. (20) can be explicitly written as

$$\begin{aligned} \bar{g}_{rr}(\mathbf{r}) &= \frac{1}{N} \sum_{m \neq n} \mathbb{E} \left[\frac{(\tilde{\mathcal{H}}_1)_{nm}(\tilde{\mathcal{H}}_1)_{mn}}{(E_n(\mathbf{r}) - E_m(\mathbf{r}))^2} \right], \\ \bar{g}_{\phi\phi}(\mathbf{r}) &= \frac{r^2}{N} \sum_{m \neq n} \mathbb{E} \left[\frac{(\tilde{\mathcal{H}}_2)_{nm}(\tilde{\mathcal{H}}_2)_{mn}}{(E_n(\mathbf{r}) - E_m(\mathbf{r}))^2} \right], \\ \text{and } \bar{g}_{r\phi}(\mathbf{r}) &= \frac{r}{N} \sum_{m \neq n} \mathbb{E} \left[\frac{(\tilde{\mathcal{H}}_1)_{nm}(\tilde{\mathcal{H}}_2)_{mn}}{(E_n(\mathbf{r}) - E_m(\mathbf{r}))^2} \right], \end{aligned} \quad (22)$$

where we have defined the following transformed operators,

$$\tilde{\mathcal{H}}_1 = \cos \phi \mathcal{H}_1 + \sin \phi \mathcal{H}_2, \quad \tilde{\mathcal{H}}_2 = -\sin \phi \mathcal{H}_1 + \cos \phi \mathcal{H}_2, \quad (23)$$

and $\mathbf{r} = \{r, \phi\}$, while $E_n(\mathbf{r})$ denotes the n -th energy of the total Hamiltonian. Note that the expression for the total Hamiltonian becomes $H = H_0 + r\tilde{\mathcal{H}}_1$, and the new variables $\tilde{\mathcal{H}}_i$ are GUE matrices having the same variance $\sigma^2 = 1/N$.

Performing an average over the ensemble of $H(\mathbf{r})$, the ensemble-averaged components of QMT can be evaluated to

be⁷ [42]

$$\bar{g}_{rr}(r) = \frac{N-1}{2(r^2+1)^2}, \quad \bar{g}_{\phi\phi}(r) = \frac{(N-1)r^2}{2(r^2+1)}, \quad \bar{g}_{r\phi} = 0. \quad (24)$$

The coordinate r takes positive values. The Ricci scalar associated with this metric can be computed easily, and it can be checked that this scalar curvature always takes the constant and positive value, $R = \frac{4}{N-1}$. Therefore, this metric essentially represents a sphere embedded in three-dimensional flat space. By explicit coordinate transformation in Appendix C, we show that the above line element can be recast into the familiar metric on S^2 .

For an ensemble with only a chaotic phase, we see that the metric components do not diverge for any values of the parameters within the allowed ranges. This can be understood from the fact that due to the presence of the level repulsion, there is always a minimum value of the energy difference. This is, e.g., different from what happens to the QMT components of the ground state of a quantum system which undergoes a quantum phase transition [9].

B. Solutions of the geodesic equations

Our goal in the rest of this section is to obtain the geodesic equations and get the first-order equations for the coordinates in terms of the conserved quantities associated with the metric components in (24). These first-order equations can then be solved for the coordinates. The solutions to the geodesic equations for the dS_2 space are well known. Here, we provide the solutions in terms of the coordinates r , and ϕ for completeness; also, these will be helpful for comparison with the solutions obtained in the next section for the metric for the Hamiltonian with integrability to chaos transition.

The geodesic equations for the metric (24) are given by

$$\begin{aligned} \frac{d^2 r}{d\lambda^2} + \Gamma_{rr}^r \left(\frac{dr}{d\lambda} \right)^2 + \Gamma_{\phi\phi}^r \left(\frac{d\phi}{d\lambda} \right)^2 &= 0, \\ \frac{d^2 \phi}{d\lambda^2} + 2\Gamma_{\phi r}^\phi \left(\frac{dr}{d\lambda} \right) \left(\frac{d\phi}{d\lambda} \right) &= 0. \end{aligned} \quad (25)$$

Here λ is a parameter which parametrises the geodesic path. For the metric components given in (24), these equations are given by

$$\ddot{r}(\lambda) - \left(\dot{\phi}^2(\lambda) + \frac{2\dot{r}^2(\lambda)}{r^2(\lambda)+1} \right) r(\lambda) = 0, \quad (26)$$

and

$$\ddot{\phi}(\lambda) + \frac{2\dot{\phi}(\lambda)\dot{r}(\lambda)}{r(\lambda)(r^2(\lambda)+1)} = 0, \quad (27)$$

⁷ We have provided a brief outline of the procedure of obtaining these metric components in Appendix B.

where, an overdot denotes a derivative with respect to the parameter λ . In general, these second-order differential equations are difficult to directly solve analytically. However, here, we can use the conserved quantities associated with the symmetries of the above metric to reduce these equations to first-order equations, which can be solved relatively easily. First, we notice that in (r, ϕ) coordinates, the components of the metric tensors are independent of ϕ , hence this is the cyclic coordinate in this case, which therefore guarantees the existence of a Killing vector and a corresponding conserved quantity along the geodesic trajectories [52]. For the metric in (24), this Killing vector is $K^a = (0, 1)$, and therefore, the conserved quantity along the geodesics associated with this Killing vector is given by

$$L = K_a \frac{dx^a(\lambda)}{d\lambda} = \frac{r^2 A}{r^2 + 1} \dot{\phi}(\lambda) = \text{constant}, \quad (28)$$

where for convenience, we have denoted $A = (N-1)/2$. Since $g_{ab} \dot{x}^a \dot{x}^b = K^2$ is also constant along the geodesic, expanding this constraint and subsequently eliminating $\dot{\phi}(\lambda)$ using eq. (28), we get the following first-order equation for $r(\lambda)$,

$$\left(\frac{dr(\lambda)}{d\lambda} \right)^2 = \frac{(r^2 + 1)^2}{A} \left[K^2 - \frac{L^2(r^2 + 1)}{Ar^2} \right]. \quad (29)$$

This equation can now be solved analytically. The expression for $r(\lambda)$ with the initial condition $r(\lambda = 0) = r_0$ is given by

$$r_{\pm}(\lambda) = \frac{1}{\sqrt{AK^2 - L^2}} \left(AK^2 \tan^2 \left[\frac{K\lambda}{\sqrt{A}} \pm C_1 \right] + L^2 \right)^{1/2}, \quad (30)$$

where, we have defined the constant $C_1 = \arctan \left(\sqrt{r_0^2 - \frac{L^2(r_0^2 + 1)}{AK^2}} \right) = \arctan C_2$ and \pm signify for initially growing ($r_+(\lambda)$) and decaying ($r_-(\lambda)$) solutions, respectively. If we concentrate only on geodesics with constant value of ϕ , then the solution for $r(\lambda)$ takes a particularly simple form of, $r_{\pm}(\lambda) = \left| \tan \left[\frac{K}{\sqrt{A}} \lambda \pm \arctan r_0 \right] \right|$.

To see the behaviour of $r(\lambda)$ for small values of the parameter λ , we expand the general solution, and for $r_0 = 1$, can write down the following expressions for $r_{\pm}(\lambda)$,

$$r_{\pm}(\lambda) \approx 1 \pm \frac{2}{A} \sqrt{AK^2 - 2L^2} \lambda + \frac{2}{A^2} (AK^2 - L^2) \lambda^2 + \mathcal{O}(\lambda^3). \quad (31)$$

Therefore, for the initially decaying solution, $r_-(\lambda)$, decays linearly for small values of λ , after which the quadratic term takes over, and $r_-(\lambda)$ starts to grow. We can obtain an analytical formula for the time when an initially decaying solution for $r(\lambda)$ bounces and starts to grow. From the expression in eq. (30) we obtain this value of the parameter to be

$$\lambda_{\text{bounce}} = \frac{\sqrt{A}}{K} \text{arccot}(1/C_2). \quad (32)$$

For the case with $L = 0$, the decaying solution reaches zero at the parameter value $\lambda = \frac{\sqrt{A}}{K} \arctan r_0$.

As can be guessed from the form of the solution for $r(\lambda)$, both $r_{\pm}(\lambda)$ diverges (or grows indefinitely) for some particular

value of λ , which for the above solutions, we can determine to be $\lambda_{\pm} = \left(\frac{\pi}{2} \mp C_1 \right) \frac{\sqrt{A}}{K}$. This indicates that, as expected, any point on the parameter manifold can be reached for a finite value of the parameter, i.e., within a finite geodesic distance.

Here we note that, the geodesic distance between two points on the state space of a quantum system is traditionally referred to as the Fubini-Study complexity.⁸ However, the geometry in (19) is not directly derived from the Provost-Valley metric associated with any generic quantum state [6].

Nevertheless, interpreting the geodesic distance associated with the metric in (19) as some notion of *complexity*, the above results indicate that one can reach any point on the parameter space with a finite value of the complexity. We also note that this feature of complexity is somewhat different from what is observed, e.g., in the parameter manifold of the quantum many-body systems with long-range interactions and shows quantum phase transition, such as the Lipkin-Meshkov-Glick model [53–55], where the separatrix connecting two different phases of the model can never be reached moving along a geodesic with finite geodesic distance⁹ [56] (see also [57] for related discussion on behaviour geodesics associated with the classical and quantum information geometry).

Using the above solutions for $r_{\pm}(\lambda)$ we can now also determine the behaviour of $\phi(\lambda)$ by integrating the relation $\dot{\phi}(\lambda) = \frac{L(r^2 + 1)}{Ar^2}$. For the initially growing and decaying solutions of $r(\lambda)$ these are given by, respectively,

$$\phi_{\pm}(\lambda) = \arctan \left(\frac{\sqrt{A}K}{L} \tan \left[\frac{K}{\sqrt{A}} \lambda \pm C_1 \right] \right) - (\phi_0)_{\pm}, \quad (33)$$

where $(\phi_0)_{\pm}$ denotes the initial values of the ϕ coordinates for two solutions. We can fix this constant in such a way that $\phi_{\pm}(\lambda = 0) = 0$. We also assume that the constant $L \geq 0$, so that the relation $\dot{\phi}(\lambda) = \frac{L(r^2 + 1)}{Ar^2}$ implies that both the solutions grows with λ .

Eliminating λ between r and ϕ we get the solution of the geodesic equation in the $r - \phi$ plane to be (for $L \neq 0$),

$$r^2 = \frac{L^2}{AK^2 - L^2} \left(\tan^2(\phi + \phi_0) + 1 \right). \quad (34)$$

IV. CORRELATION FUNCTION OF GUE MATRICES AND THE FIDELITY SUSCEPTIBILITY

As we have discussed in section II A, the components of the ensemble-averaged QMT are closely related to the two-point connected correlation functions of the relevant operators. To understand this connection more closely in the context of random matrix Hamiltonians, in this section, we compute the correlation function of the form $\langle \mathcal{H}(t) \mathcal{H} \rangle$ that appears

⁸ To be more precise, this is the complexity defined on the parameter manifold with the Fubini-Study metric pulled-back from the state space, equipped with a coordinate chart defined by the parameters of the system.

⁹ We remind the reader that in the latter case of quantum many-body systems, usually the Fubini-Study complexity refers to the geodesic distance between two points on the space of pure quantum states, such as the ground or the first excited state.

in (14), with the time evolution generated by a Hamiltonian of the type in (1). Then we shall show how one can recover the expressions of the FS from this correlation function, thereby illuminating the important role played by the correlation between the energy levels in determining the behaviour of the geometry of the eigenstates.

In this section, we first evaluate the correlation function by scaling the total Hamiltonian¹⁰ as $\tilde{H} = H/\alpha$, where $\alpha = \sqrt{(r^2 + 1)\sigma}$, where σ^2 is the variance of the matrices H_0 and \mathcal{H} , both drawn from independent GUE. Hence, the Hamiltonian we consider is,¹¹

$$\tilde{H} = \frac{1}{\alpha}(H_0 + V) = \frac{1}{\alpha}(\sigma\tilde{H}_0 + \sigma r\tilde{V}), \quad (35)$$

$$V = r\mathcal{H}, \quad \mathbb{E}(|(H_0)_{ij}|^2) = \mathbb{E}(|(\mathcal{H})_{ij}|^2) = \sigma^2,$$

whereas, the correlation function we are interested in computing is the following,

$$\tilde{G}(t) = \langle V(t)V \rangle = r^2 \langle \mathcal{H}(t)\mathcal{H} \rangle = r^2 \sigma^2 \langle \tilde{V}(t)\tilde{V} \rangle, \quad (36)$$

where $O(t) = e^{it\tilde{H}} O e^{-it\tilde{H}}$.

Note that we have defined rescaled matrices $\tilde{H}_0 = H_0/\sigma$ and $\tilde{V} = V/(r\sigma)$, each of which has unit variance (and zero mean), and the ensemble average is over the following probability distribution

$$P(H_0, \mathcal{H}) = Z^{-1} \exp \left[-\frac{1}{2\sigma^2} (\text{Tr}(H_0^2) + \text{Tr}(\mathcal{H}^2)) \right], \quad (37)$$

where Z is a normalisation constant.

Before moving on to the computation of this correlation function, we note a difference between this and similar ensemble-averaged two-point correlation functions usually considered in the random matrix literature. Here, the operator V , whose correlation function we want to obtain itself belongs to the ensemble with respect to which the average is performed. This is different from, e.g., the situation considered in [58], where the ensemble-averaged two-point functions of operators that do not belong to the ensemble were obtained. In this case, the resulting two-point function can be related to the two-point SFF. Here we want to see whether it is possible to relate the correlation function in (36) to the SFF.

To obtain the correlation function $\tilde{G}(t)$ in (36), we start by noting that the probability distribution in Eq. (37) is not factorised when written in terms of the variable \tilde{H} and \mathcal{H} . The strategy we use in the following is to find a new variable, say X , so that we can write the probability distribution in a factorised form in terms of \tilde{H} and X . For this purpose, we first

perform the substitution $H_0 = \alpha\tilde{H} - r\mathcal{H}$ and, after a bit of manipulation, see that it can be written as

$$P(\tilde{H}, X) = Z^{-1} \exp \left[-\frac{1}{2} (\text{Tr}(\tilde{H}^2) + \text{Tr}(X^2)) \right], \quad (38)$$

where the desired variable X is given by

$$X = \frac{1}{\sigma} (\sqrt{r^2 + 1}\mathcal{H} - r\sigma\tilde{H}) = \frac{1}{\sqrt{r^2 + 1}} (\tilde{V} - r\tilde{H}_0). \quad (39)$$

Thus, the random variables X and \tilde{H} are independent of each other. It can be straightforwardly checked that, similar to \tilde{H} , the average variance of the elements X is unity, i.e. $\mathbb{E}(|X_{ij}|^2) = 1$. Next, we perform these variable changes in the ensemble averaging, namely, $\{H_0, \mathcal{H}\} \rightarrow \{\tilde{H}, X\}$. Hence, the correlation function under consideration becomes,

$$\begin{aligned} \tilde{G}(t) &= \frac{r^2}{NZ} \int \text{Tr} \left[(C_1 X(t) + C_2 \tilde{H}) (C_1 X + C_2 \tilde{H}) \right] P(\tilde{H}, X) d\tilde{H} dX \\ &= C_1^2 \langle X(t)X \rangle + 2C_1 C_2 \langle X\tilde{H} \rangle + C_2^2 \langle \tilde{H}^2 \rangle, \end{aligned} \quad (40)$$

where $C_1 = \sigma/\sqrt{r^2 + 1}$ and $C_2 = (r\sigma)/\sqrt{r^2 + 1}$. Note that the constant factors coming from the Jacobians of the transformations cancel from the corresponding factors in the denominator. Using the fact that the mean and variance of both the variables (X and \tilde{H}) are 0 and 1, respectively, it is easy to check that $\langle X\tilde{H} \rangle = 0$ and $\langle \tilde{H}^2 \rangle = N$. Finally, the first term in the second line of the expression can be checked to be related to the spectral form factor by the relation, $\langle X(t)X \rangle = \frac{\tilde{R}(t)}{N}$, where we have defined the SFF as

$$\tilde{R}(t) = Z^{-1} \int |\text{Tr}(e^{-i\tilde{H}t})|^2 P(\tilde{H}) d\tilde{H}. \quad (41)$$

Collecting all these results, the final expression for the correlation function $\tilde{G}(t)$ is given by

$$\tilde{G}(t) = \frac{r^2 N \sigma^2}{r^2 + 1} \left(\frac{\tilde{R}(t)}{N^2} + r^2 \right). \quad (42)$$

In Appendix D, we provide an alternative method to evaluate this correlation function which utilises the fact that in the limit $N \rightarrow \infty$, one can find a variable which is free from \tilde{H} , and hence compute the correlation function using tools of free probability. These two analytical expressions, along with the numerically obtained result for the correlator $\tilde{G}(t)$ are shown in Fig. 1. As can be seen from this plot, the analytical expression in (42) shows an excellent agreement with the numerical result.

A. Fidelity susceptibility from correlation function

We now discuss the procedure of recovering the expression for the FS from the expression for the correlation function by employing the formula in (11). First, we provide the expression for $G(t)$ without scaling the Hamiltonian, i.e. for the one

¹⁰ The scaling is performed to make the connection with an alternative method of evaluating the correlation function presented in Appendix D manifest. Towards the end of this section we provide the expression for the correlation function appearing in (14) for the non-scaled Hamiltonian.

¹¹ In terms of the notation used in section III, $\mathcal{H} = \mathcal{H}_1$. To keep the discussion simple, here we assume that the total Hamiltonian depends on only one parameter r . Therefore, the FS one would get here is the same as the rr component of the QMT in (24).

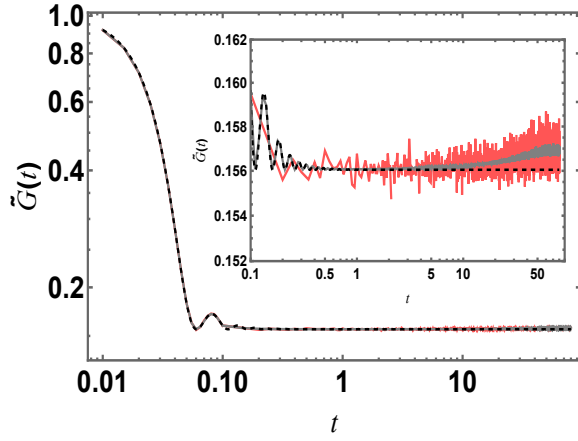


FIG. 1. Plot of the correlation function $\tilde{G}(t) = \langle H(t)H \rangle$ (in the Log-Log scale), where the time evolution is generated by the rescaled Hamiltonian (35). Here $N = 1000$, $r = 0.43$, and the plot shows the result with an average over 100 independent realisations of the Hamiltonian \tilde{H} . The red curve denotes the numerical result, while $\tilde{G}(t)$ computed from the formulas in (42) and (D4), are respectively shown by the grey, black dashed curves. The plot in the inset shows, more closely, the behaviour of the correlation function at late times (with the same colour coding) and the difference between these two analytical expressions. This difference would be negligible in the limit $N \rightarrow \infty$.

in (14), where the time-evolution is generated by the Hamiltonian in (1). By following a similar analysis to the one presented above, we obtain the expression for the required correlation function to be

$$G(t) = \frac{1}{(r^2 + 1)} \left(\frac{\mathcal{R}(t \sqrt{r^2 + 1})}{N^2} + r^2 \right), \quad (43)$$

where $\mathcal{R}(t)$ now denotes the SFF associated with $H(r)$, i.e.,

$$\mathcal{R}(t) = \frac{1}{Z'} \int |\text{Tr}(e^{-iH't})|^2 P(H') dH', \quad H' = \frac{H}{\sqrt{r^2 + 1}}, \quad (44)$$

Z' is a constant that normalises the distribution $P(H')$. Note that H' is a random matrix drawn from a GUE with variance σ^2 .

To obtain the expression for the FS, we first note that, from the definition of SFF, we have,

$$\mathcal{R}(t') = N + \int \mathcal{D}E' \sum_{i \neq j} e^{i(E'_i - E'_j)t'}. \quad (45)$$

Here E'_i denotes the eigenvalues of the matrix H' , $t' = t \sqrt{r^2 + 1}$, and $\mathcal{D}E'$ denotes the average over the ensemble, when written in terms of the eigenvalues, i.e., written in terms of the joint probability distribution eigenvalues of H' (e.g., using the distribution in (6)). Now substituting this expression in (43), and subsequently using it in (9) we get

$$\bar{g}_{rr}(r) = \frac{1}{N^2(r^2 + 1)} \sum_{i \neq j} \int \mathcal{D}E' \int_{-\infty}^{\infty} \frac{d\omega}{\omega^2} \int_{-\infty}^{\infty} \frac{dt}{2\pi} e^{i\omega t} e^{i(E'_i - E'_j)t'}, \quad (46)$$

here we have used the fact that $N^{-1} \mathbb{E} \sum_n |\langle n | H | n \rangle|^2 = (1 + Nr^2)/(N(r^2 + 1))$ in (12). A straightforward computation shows that we get back the expression for the FS,

$$\bar{g}_{rr}(r) = \frac{1}{N^2(r^2 + 1)^2} \sum_{i \neq j} \int \mathcal{D}E' \frac{1}{(E'_i - E'_j)^2} = \frac{N - 1}{2(r^2 + 1)^2}, \quad (47)$$

where, in the last step, we have used the virial relation in eq. (B4) along with the fact that here $\sigma_\star^2 = N^{-1}$. One can follow a similar procedure to obtain the other components of the QMT from other relevant correlation functions.

Before concluding this section, we note the following points. The initial decaying part of the SFF comes from the disconnected piece of the 2-point spectral correlation function $\rho^{(2)}(E'_1, E'_2)$ [59, 60], which in turn, produces the N -independent term $\frac{-1}{2(r^2 + 1)^2}$ in the FS. To see this, we note that the contribution of the disconnected part to the FS can be written as,

$$\bar{g}_{rr}^c(r) = \frac{1}{(r^2 + 1)} \int_{-\infty}^{\infty} \frac{dt}{2\pi} e^{i\omega t} \int_{-\infty}^{\infty} \frac{d\omega}{\omega^2} |\langle e^{-it'H'} \rangle|^2, \quad (48)$$

where the connected part of the SFF is given by

$$\langle e^{-it'H'} \rangle = \frac{1}{N} \sum_i \int \mathcal{D}E' e^{-E'_i t'} = \int dE' \rho(E') e^{-iE' t'}. \quad (49)$$

Here $\rho(E')$ is the density of states of H' , with the integral being over the support of $\rho(E')$ on the real line. The last two expressions can be combined to get

$$\bar{g}_{rr}^c(r) = \frac{1}{(r^2 + 1)^2} \int dE'_1 dE'_2 \frac{\rho(E'_1) \rho(E'_2)}{(E'_1 - E'_2)^2}. \quad (50)$$

To evaluate the last integral, we utilise the resolvent of H' , (which is just the Cauchy transformation of the density of states), defined as

$$G_{H'}(x) = \int \frac{\rho(E')}{x - E'} dE'. \quad (51)$$

Now we can write $\bar{g}_{rr}^c(r)$ as

$$\bar{g}_{rr}^c(r) = -\frac{1}{(r^2 + 1)^2} \int dE'_1 \rho(E'_1) \frac{dG_{H'}(E'_1)}{dE'_1}. \quad (52)$$

Finally, using the well-known expression for the resolvent for GUE Hamiltonians (with variance $\sigma^2 = 1/N$) (see e.g., [31, 61, 62]),

$$G_{H'}(x) = \frac{1}{2} (x - \sqrt{x^2 - 4}), \quad (53)$$

we get $\bar{g}_{rr}^c(r) = -\frac{1}{2(r^2 + 1)^2}$, which is N -independent part of the FS in (47).

On the other hand, the connected part of the 2-point spectral correlation function $\rho^{(2)}(E'_1, E'_1)$ (given by the so-called sine kernel for GUE Hamiltonians), which gives rise to the ramp in SFF, gives the other part (which N -dependent, therefore, extensive) of the FS in (47). The last two points clearly

illustrate the role played by the correlation between the eigenvalues in the QMT components.

Since the correlation function $G(t)$ is related to the FS, the relation in (43) provides a direct connection of the SFF, one of the most commonly used tools to study quantum chaos, to the FS. It will be interesting to see whether such a relationship can be established for a more generic class of ensembles, such as the RP model, which breaks the rotational invariance of the classical Gaussian ensembles considered in this section.

V. GEOMETRIC PROPERTIES OF QUANTUM METRIC TENSOR FOR INTEGRABILITY BREAKING HAMILTONIAN

As we have discussed in the Introduction, one of the main focuses of this paper is to study the geometry of quantum energy eigenstates of systems that show chaos-to-integrability transitions. For this purpose, in this section, we begin by considering the eigenstate space geometry of a Hamiltonian which can be written in the following way,

$$H(r, \phi) = H_0 + r \cos \phi \mathcal{H}_1 + r \sin \phi \mathcal{H}_2, \quad (54)$$

which is of the same form as the one considered in the previous section (eq.(21)), however, here the matrix H_0 is taken to be a diagonal matrix whose elements are drawn independently from Gaussian distributions with mean zero and unit variance. This Hamiltonian can be thought of as a generalisation of the standard RP model [33].

A. QMT of a 2×2 Integrability breaking Hamiltonian

Even though the limit $N \rightarrow \infty$ is usually more interesting compared to finite N for random matrix theories, in many situations, finite N cases can also provide interesting insights into different properties of the random matrix ensemble. In fact, conclusions obtained from the smallest matrix with size $N = 2$ can have very useful information about their higher N generalisations, one example being the famous Wigner's surmise of the level spacing distribution of random matrix eigenvalues, which is derived from $N = 2$ matrices, and is actually an excellent approximation of the level spacing distribution of larger matrices [61] (see also [63] and reference cited therein).

In this spirit, a two-parameter family of 2×2 random matrices, where two GUE matrices are added to a random diagonal integrable matrix, was used in [42] to obtain an exact analytical expression for the components of the ensemble-averaged QMT. Specifically, the Hamiltonian is of a similar structure as that of the one in (21), where H_0 is a diagonal matrix whose elements are independent and identically distributed Gaussian random variables. Below, we use this QMT to study its various geometric properties, such as the scalar curvature invariants and the structure of the geodesics in this geometry.

The line element corresponding to the ensemble-averaged QMT obtained from a 2×2 matrix representation of the integrability-breaking Hamiltonian in (54) is given in the $\{r, \phi\}$

coordinates by the following expression¹² [42]

$$ds^2 = \tilde{g}_{rr} dr^2 + \tilde{g}_{\phi\phi} d\phi^2, \quad (55)$$

where $\tilde{g}_{rr}(r) = \frac{1}{4} \left(\frac{1}{\sqrt{2}r} \operatorname{arccot}(r/\sqrt{2}) - \frac{1}{2+r^2} \right),$

and $\tilde{g}_{\phi\phi}(r) = \frac{r}{2\sqrt{2}} \arctan(\sqrt{2}/r).$

A derivation of the rr component of this line element from a real symmetric tridiagonal matrix representation of the GUE is presented in the section VIA.

With the above line element in hand, first, consider two different limits of these metric components. In the limit $r \rightarrow 0$ (which corresponds to the limit where the Hamiltonian is completely integrable), it can be easily checked that the rr component diverges, while the $\phi\phi$ component goes to zero. On the other hand, in the limit, $r \rightarrow \infty$ (this corresponds to the case where the Hamiltonian is far away from the integrable phase), \tilde{g}_{rr} vanishes, but $\tilde{g}_{\phi\phi}$ takes a constant value $1/2$.

Next, we consider the Ricci scalar associated with this metric. The expression for the Ricci scalar in terms of the (r, ϕ) coordinates is given by,

$$\tilde{R} = \frac{4\sqrt{2}r - 4(r^2 - 2)\operatorname{arccot}(r/\sqrt{2})}{(r^2 + 2)\operatorname{arccot}^2(r/\sqrt{2})((r^2 + 2)\operatorname{arccot}(r/\sqrt{2}) - \sqrt{2}r)}. \quad (56)$$

As can be expected, in contrast to the previous case of a random matrix Hamiltonian, the Ricci scalar is not a constant but varies with r . For large values of r , i.e., far away from integrability, we can write down the following expansion of the Ricci scalar,

$$\tilde{R} = 4 - \frac{64}{15r^2} + \frac{3904}{525r^4} + \mathcal{O}(r^{-6}). \quad (57)$$

Therefore, as one moves from integrability by increasing the value of r , the value of the Ricci scalar increases and subsequently attains a constant positive value of 4, consistent with the discussion of the previous section. Also note that as one decreases r , the Ricci scalar monotonically decreases, and in the limit $r \rightarrow 0$, it attains a constant positive value $8/\pi^2$. The Ricci scalar is regular for all admissible values of the parameter r , indicating that there is no curvature singularity in the geometry. We have shown a plot of the Ricci scalar in Fig. 2.

B. Solutions of the geodesic equations

We now proceed to obtain the geodesic curves for the metric in (55). We first notice that, for the metric in (55) as well,

¹² We use a tilde to distinguish the new quantities for the metric in (55) from the analogous quantities for the random matrix case discussed in the previous section. However, to avoid cluttering the notation, we have removed the bar indicating an ensemble average.

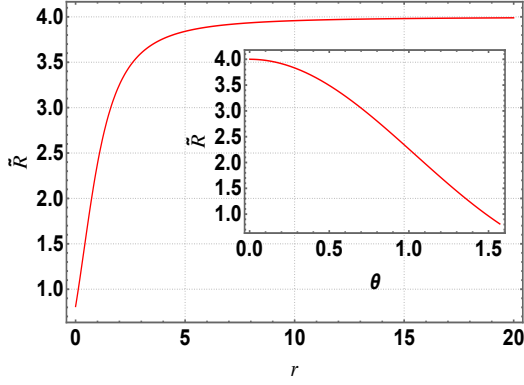


FIG. 2. Plot of the Ricci scalar for the QMT associated with the 2×2 integrability-breaking Hamiltonian. For large values of the coordinate r , the Ricci scalar approaches a constant value of 4, and always remains positive for all the allowed range of the r parameter. The plot in the inset shows the variation of \tilde{R} as a function of the coordinate θ , where $r = \sqrt{2} \cot \theta$. $\theta = 0$ corresponds to the limit $r \rightarrow \infty$, while $r = 0$ is mapped to $\theta = \pi/2$.

ϕ is a cyclic coordinate. Hence, we can obtain the conserved quantity associated with the Killing vector $K^a = (0, 1)$ to be¹³

$$\tilde{L} = \frac{r}{2\sqrt{2}} \arctan(\sqrt{2}/r) \dot{\phi}(\lambda). \quad (58)$$

Once again using the fact that $\tilde{g}_{ab} \dot{x}^a \dot{x}^b = \tilde{K}^2$, with \tilde{K} being a constant and $x^a = \{r, \phi\}$, the first order equation for $r(\lambda)$ we obtain is given by

$$\left(\frac{dr(\lambda)}{d\lambda} \right)^2 = 4 \left[\tilde{K}^2 - \tilde{L}^2 \left(\frac{r}{2\sqrt{2}} \arctan(\sqrt{2}/r) \right)^{-1} \right] \left(\frac{1}{\sqrt{2}r} \operatorname{arccot}(r/\sqrt{2}) - \frac{1}{2+r^2} \right)^{-1}. \quad (59)$$

It is difficult to solve this equation in general. For this purpose, we first make a coordinate transformation that will simplify the metric components as well as the first-order geodesic equations. Consider the following transformation of the r coordinate, $r = \sqrt{2} \cot \theta$, such that the line element, after this coordinate change, becomes,

$$ds^2 = \frac{1}{4} \left(\frac{2\theta}{\sin 2\theta} - 1 \right) \operatorname{cosec}^2 \theta d\theta^2 + \frac{1}{2} \theta \cot \theta d\phi^2. \quad (60)$$

Note that, in terms of the coordinate θ , the integrable limit of the Hamiltonian corresponds to $\theta = \pi/2$, while as one breaks the integrability by increasing the parameter r , the value of θ decreases, and the limit $r \rightarrow \infty$ corresponds to $\theta = 0$.

The conserved quantity \tilde{L} in the coordinates (θ, ϕ) takes the form

$$\tilde{L} = \frac{1}{2} \theta(\lambda) \cot \theta(\lambda) \dot{\phi}(\lambda). \quad (61)$$

Substituting $\dot{\phi}(\lambda)$ from this relation in the expression $\tilde{g}_{ab} \dot{x}^a \dot{x}^b = \tilde{K}^2$, we get the first-order expression for $\dot{\theta}(\lambda)$ to be

$$\dot{\theta}(\lambda)^2 = 4 \sin^2 \theta \left[\tilde{K}^2 - \tilde{L}^2 \frac{2}{\theta} \tan \theta \right] \left(\frac{2\theta}{\sin 2\theta} - 1 \right)^{-1}. \quad (62)$$

We first provide numerical solutions to the above equation for two cases, when the $\dot{\theta}(\lambda)$ is positive and when it's negative. Then we will analyse an approximate analytical solution of this equation, which, as we shall show, provides a good approximation of the numerical results.

In Fig. 3, we have shown the numerical solutions of the first-order equation for $\theta_0 = \theta(\lambda)$ for three different initial values of $\theta(\lambda = 0)$. Here we have plotted the solutions for which $\dot{\theta}(\lambda)$ is positive, i.e., the solutions are initially expanding. From the plots, we see that these initially expanding geodesics, starting from a point arbitrarily away from $\theta = \pi/2$ on the parameter space, asymptotically reach the integrable phase corresponding to $\theta = \pi/2$.

On the other hand, for the decaying class of solutions, plotted in Fig. 4, $\theta(\lambda)$, for different initial values θ_0 , reach to the constant value of zero (the lower limit of the range of the coordinate θ) for specific values of λ . This indicates that, starting from a point in the parameter space corresponding to a slight breaking of integrability (small value of the parameter r , θ close to $\pi/2$), one can follow an initially decaying geodesic trajectory to reach a point far away from the integrability in a finite value of the affine parameter λ .

Next, we show that it is possible to perform an analytical approximation of the geodesic equation for small values of θ , so that one can obtain an analytical expression for $\theta(\lambda)$. To this end, we expand the right-hand side of the eq. (62) for small values of θ , and keeping terms up to $O(\theta^2)$ we obtain (for an initially decaying geodesic)

$$\dot{\theta}(\lambda) \approx -(A_1 + A_2 \theta(\lambda)^2), \quad (63)$$

¹³ To distinguish from the conserved quantity L of the previous section, here we have denoted the conserved quantity associated with the cyclic coordinate ϕ to \tilde{L} .

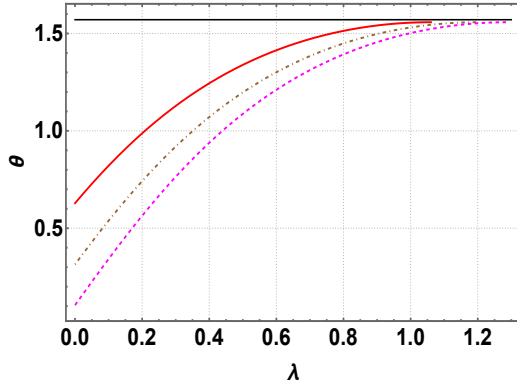


FIG. 3. Plot of $\theta(\lambda)$ for three different initial values of θ : $\theta_0 = \pi/5$ (red), $\theta_0 = \pi/10$ (brown), $\theta_0 = \pi/30$ (magenta). The dashed black line indicates the upper limit $\theta = \pi/2$. Here, we have fixed $\tilde{K} = 1$, and $\tilde{L} = 0.1$ in all three plots. For these solutions, $\theta(\lambda)$ grows initially.

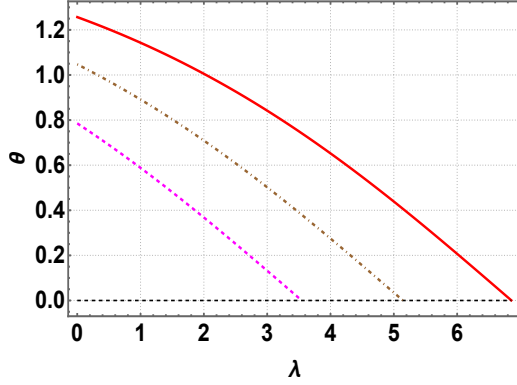


FIG. 4. Plot of $\theta(\lambda)$ for three different initial values of θ : $\theta_0 = 2\pi/5$ (red), $\theta_0 = \pi/3$ (brown), $\theta_0 = \pi/4$ (magenta). The dashed black line indicates the lower limit $\theta = 0$. Here, we have fixed $\tilde{K} = 0.1$, and $\tilde{L} = 0.1$ in all three plots. For these solutions, $\theta(\lambda)$ s represent initially decaying solutions.

where we defined two constants, $A_1 = \sqrt{6(\tilde{K}^2 - 2\tilde{L}^2)}$ and $A_2 = \sqrt{\frac{2}{3} \frac{7\tilde{L}^2 - 6\tilde{K}^2}{\tilde{K}^2 - 2\tilde{L}^2}}$. This equation can be easily solved to obtain the following expression for $\theta(\lambda)$ (with the initial condition $\theta(\lambda = 0) = \theta_0$),

$$\theta(\lambda) = -\sqrt{\frac{A_1}{A_2}} \tan \left[\sqrt{A_1 A_2} \lambda - \arctan \left(\sqrt{\frac{A_2}{A_1}} \theta_0 \right) \right]. \quad (64)$$

In Fig. 5 we have shown a comparison of the approximate expression (64) with the numerically obtained solution. As can be seen, the solution in eq. (64) actually provides quite a good approximation to the numerical solution for the entire range of θ . For comparison, we have also plotted a simple linear expression $\theta(\lambda) \approx A_1(c - \lambda)$, with c being a constant, which shows that close to $\theta = 0$ (far away from the integrable phase), the geodesic solution $\theta(\lambda)$ linearly goes to zero.

Finally, from the expression for $\theta(\lambda)$ in (64) we can obtain

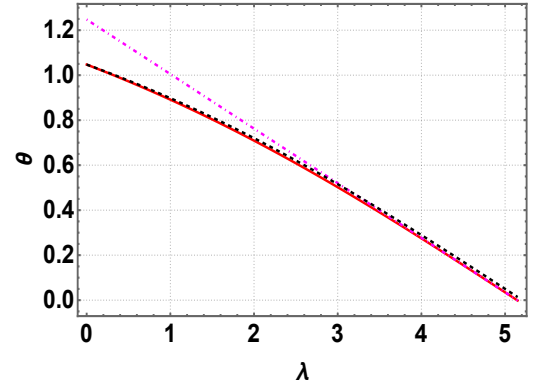


FIG. 5. Comparison of the numerical solution of $\theta(\lambda)$ (red curve) with the approximate solution in eq. (64) (shown by black dashed curve). We have fixed $\tilde{K} = 0.1$, $\tilde{L} = 0.1$, and $\theta_0 = \pi/3$. The dot-dashed magenta line represents an approximate linear solution close to $\theta = 0$.

an expression for $r(\lambda)$, given by

$$r(\lambda) = -\sqrt{2} \cot \left(\sqrt{\frac{A_1}{A_2}} \tan \left[\sqrt{A_1 A_2} \lambda - \arctan \left(\sqrt{\frac{A_2}{A_1}} \theta_0 \right) \right] \right). \quad (65)$$

As can be seen by expanding this expression, for small values of the parameter λ , $r(\lambda)$ grows linearly, after which quadratic growth takes over. This expression, along with $r(\lambda)$ obtained using the numerical solution for $\theta(\lambda)$ is plotted in Fig. 6 for two different initial values of r_0 . The approximate expression in (65) is in good agreement with the numerical solution for both the initial conditions. Furthermore, from this solution for $r(\lambda)$ we once again see that one can reach any arbitrary value of r , for a finite value of the parameter λ following this geodesic. Therefore, any point arbitrarily far away from the integrable phase can be reached with a finite distance, i.e., a finite value of the 'complexity'.

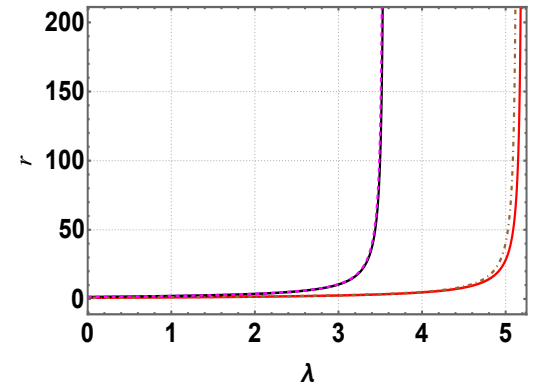


FIG. 6. Comparison of the numerical solution of $r(\lambda)$ (red and black curves, with $r_0 = \sqrt{2/3}$ and $r_0 = \sqrt{2}$, respectively) with the approximate solution in eq. (65) (shown by brown and magenta dashed curves with the same initial conditions). We have set $\tilde{K} = 0.1$, $\tilde{L} = 0.1$.

Before concluding this section we note that here we have

performed an analysis of different geometric quantities for the generalised version of the conventional RP model with $N = 2$. While it would be very much desirable to perform a similar analysis for a generic N , analytic expressions for the QMT components for an arbitrary value of N are not known. In [42], these components were obtained numerically, and it was shown that the metric components follow different scaling properties in different phases of this model. E.g., when $r \ll r^* = 1/\sqrt{N}$ (corresponding to the localised phase of the model), the metric components follow a $1/r$ scaling, while in the ergodic phase, having $r \gg 1$, the metric components approach those of the GUE random matrix expressions in (24). Finally, in the non-ergodic extended phase ($r^* \ll r \ll 1$), the components \tilde{g}_{rr} and $\tilde{g}_{\phi\phi}/r^2$ goes to constants scaling as N .

VI. GEOMETRY OF QUANTUM STATES FOR GAUSSIAN β -ENSEMBLES

In this section, and the next, we consider a generalization of the integrability-breaking Hamiltonian considered in the previous section, such that the Dyson index (β) can take a range of real positive values, not just those of classical Gaussian ensembles. Specifically, in this section, we consider the tridiagonal matrix representation of the so-called Gaussian β -ensembles, found in [40], a Hamiltonian belonging to the ensemble takes a real symmetric tridiagonal $N \times N$ matrix whose diagonal elements (denoted as a_n , $n = 0, \dots, N-1$) are independent Gaussian random variables with mean 0, and variance as that of the ensemble, while the sub-diagonal elements (which we call b_n , with $n = 1, \dots, N-1$) are independently distributed random variables with the following distribution

$$p(b_n) = \frac{2}{\Gamma(k/2)} \left(\frac{\beta N}{2} \right)^{k/2} b_n^{k-1} e^{-\beta N b_n^2/2}, \quad (66)$$

where $k = (N-n)\beta$. The joint probability distribution of the eigenvalues matches that of the one in eq. (6), with $V(H) = H^2$ and β taking any real positive value. Note that, unlike the three classical Gaussian ensembles, the Gaussian β -ensemble does not have rotational invariance. For a collection of works that studied different properties of the Gaussian β -ensembles, we refer to [64–68].

A natural property of the ensemble of Hamiltonians with general β is that, by controlling the value of the Dyson index, one can control the strength of the repulsion between the energy levels. In the limit $\beta \rightarrow 0$, the energy levels can be arbitrarily close to each other without any level repulsion, and therefore the level spacing statistics is Poissonian, associated with integrable systems. Increasing the value of β from this value, one gradually gets ensembles with different degrees of level repulsion, including those of the classical Gaussian ensembles (with $\beta = 1, 2, 4$), as well as ensembles having intermediate values of β . Therefore, the Gaussian β -ensembles can be thought to be showing a chaos-to-integrability transition as β is decreased below the GUE value ($\beta = 1$) towards zero. Similar to the RP model, apart from the chaos to integrability transition, the β -ensembles also show Anderson localisation

transition for a specific value of the Dyson index. Rewriting $\beta = N^\gamma$ for some real parameter γ , it has been shown recently that β -ensembles have three different phases, respectively, an ergodic phase ($\gamma \leq 0$), a nonergodic extended phase (for $0 < \gamma < 1$) and a localised phase when $\gamma \geq 1$ [69].

An important difference between the tridiagonal form of the Gaussian β -ensembles and the classical Gaussian ensembles is that the properties of the eigenvectors of the respective ensembles are quite different, even though both can have the same joint probability distribution of the eigenvalues. E.g., as a direct consequence of the rotational invariance of the probability distribution, the eigenvectors of, say, GOE are uniformly distributed on the surface of N -dimensional unit sphere and have components which are mutually independent. On the other hand, let T be a tridiagonal matrix, and $T = Q\Lambda Q^T$ be the eigendecomposition of T , with Λ denoting the diagonal matrix constructed from the eigenvalues (λ) of T , then one can show that it is possible to uniquely reconstruct the matrices T and Q starting from the eigenvalues of T and the first row of the matrix Q [40, 70].

For these ensemble with generic Dyson index, one can follow two different procedures to move to the integrable phase: 1. first, as was the case in section III, we can add a term proportional to random matrix drawn from an ensemble with a fixed general value of the Dyson index $\beta > 1$ to a diagonal matrix having independent random variables as the entry. As one takes the proportionality constant (denoted as r) to zero the total Hamiltonian makes a transition from chaotic to integrable phase as $r \rightarrow 0$. 2. Secondly, we can consider a Hamiltonian which is a sum of two terms each of which taken from these generalised β -ensembles and have, in general, different Dyson indices (β_1 and β_2). Then, as one takes either or both of these β_i close zero and take $r \rightarrow 0$, the total Hamiltonian again makes a transition from chaotic to integrable phase.

In this section, we follow the first option, i.e., we take a rank-2 matrix sampled from the tridiagonal Gaussian β -ensembles, add it to a diagonal integrable Hamiltonian, and derive the corresponding ensemble-averaged FS (which is the rr component of the line element in (55)).¹⁴ We first compute this for the case with $\beta = 2$, and show that it matches with the expression in (55), and subsequently generalise the results to obtain the ensemble-averaged FS for a generic value of $\beta > 1$.¹⁵

A. Fidelity susceptibility for tridiagonal Gaussian β -ensembles

We now derive the rr component of the line element from the tridiagonal representation of the classical Gaussian β -ensembles. We consider a system whose total Hamiltonian

¹⁴ One reason for following this procedure is that, as we shall see, the integral for the FS does not converge for the tridiagonal Hamiltonian when $\beta < 1$.

¹⁵ In the next section VII, we have provided the computation of the FS of a class of random matrices with general Dyson index, which, in contrast to the tridiagonal form used in this section, is rotationally invariant. Also in Appendix E we present a computation of the FS for a random matrix ensemble with a generic Dyson index β .

is given by the one in eq. (54) where r is a positive parameter, and H_0 is a diagonal ‘integrable’ Hamiltonian whose elements are independent random variables drawn from the distribution $\rho(x)$, and \mathcal{H} is a Hamiltonian that we sample from the Gaussian β -ensemble.

One difference from the situation considered in the two previous sections is that here we are considering the simplest situation where the total Hamiltonian H has only one parameter r , rather than both r and ϕ . Hence, in this case, the line element will consist of a single element, which is the fidelity susceptibility associated with the parameter r . The QMT components in such a situation are evaluated numerically in the next subsection.

For our purposes, it is sufficient to consider a system with a Hamiltonian of the form $H = H_0 + r \mathcal{H}_\beta$ where H_0 is a diagonal ‘integrable’ Hamiltonian, i.e., we assume that its eigenvalues are drawn from independent Gaussian distributions with zero mean and variance 1, and \mathcal{H}_β is a ‘tridiagonal’ matrix.

Therefore, we take \mathcal{H}_β to be the following 2×2 matrix

$$\mathcal{H}_\beta = \begin{pmatrix} a_0 & b_1 \\ b_1 & a_1 \end{pmatrix}. \quad (67)$$

and assume that H_0 takes the following diagonal form in the same basis

$$H_0 = \begin{pmatrix} h_1 & 0 \\ 0 & h_2 \end{pmatrix}, \quad (68)$$

where h_1 and h_2 are sampled from independent Gaussian distributions.

The Hamiltonian $H = H_0 + r \mathcal{H}_\beta$ can be thought of as the generalisation of the usual RP model (which is usually defined with \mathcal{H} taken from the classical Gaussian β -ensembles) for general values of β . (citations) The expression for g_{rr} , averaged over the ensemble is given by,

$$\bar{g}_{rr}(r, \beta) = \frac{1}{2\pi} \int \frac{\mathcal{H}_{12}\mathcal{H}_{21}}{(E_n - E_m)^2} e^{-\frac{1}{2}\text{Tr}(H_0^2)} p(a_0)p(a_1)p(b_1) dH_0 da_0 da_1 db_1. \quad (69)$$

Here $\mathcal{H}_{mn} = \langle m | \mathcal{H}_\beta | n \rangle$, are the matrix elements of \mathcal{H}_β in the energy eigenbasis of the total Hamiltonian. Note that the matrix elements \mathcal{H}_{12} and \mathcal{H}_{21} are zero if for a realisation of the matrix H_β the condition $h_1 = h_2$ is satisfied.

Case.1: $\beta = 2$. First, consider the case of $\beta = 2$. Using the expression for the distributions of a_n , and b_n s with $\beta = 2$ we get

$$\bar{g}_{rr}(r, \beta = 2) = \frac{1}{16\pi^2 r} \int \frac{b_1^3(z_1 + z_2)^2}{(4b_1^2 r^2 + z_1^2)^2} \exp\left(-\frac{1}{16}(32b_1^2 + 4x_1^2 + 8y_1^2 + \frac{2}{r^2}(z_1 - z_2)^2 + (z_1 + z_2)^2)\right) dy_1 dz_1 dz_2 dx_1 db_1, \quad (70)$$

where we have performed the following coordinate transformations,

$$\begin{aligned} h_{1,2} &= (x_1 \pm x_2)/2, \quad a_{0,1} = (y_1 \pm y_2)/2, \\ x_2 &= (z_1 + z_2)/2, \quad y_2 = (z_1 - z_2)/(2r). \end{aligned} \quad (71)$$

A difference one should notice between this integral and the usual one we get from a complex Hermitian representation of the GUE is that, for the above integral, since all the matrix elements are real, the extra factor that comes from the radial part of the complex variable in a complex Hermitian representation (see e.g., the integral in (82)) here comes from the distribution (66) of the sub-diagonal elements itself. This is

due to the fact that, like b_1 , the distribution of the radial part can be thought of as the distribution of the square root of the sum of two squared independent Gaussian variables, hence a chi distribution.

Performing the integrals in (70), we get back the expression for the rr component in (55). One can similarly derive the $\phi\phi$ component of the metric, however, in that case one needs to consider a more general Hamiltonian than $H = h_0 + r \mathcal{H}_\beta$, as in [42].

Case 2: Generic values of the Dyson index. The tridiagonal matrix representation is particularly suitable for obtaining the FS for a Gaussian ensemble with a generic value of the Dyson index for $\beta > 1$. For any $\beta > 1$, the analytical expression for $\bar{g}_{rr}(r)$ we get from (69) is given by

$$\bar{g}_{rr}(r, \beta) = \frac{\beta}{16(\beta + r^2)^2} \left[\left(\frac{r^2}{\beta} + 1 \right)^{\beta/2} (\beta + (\beta - 1)r^2) \left\{ \frac{\sqrt{\pi\beta} \Gamma(\frac{\beta-1}{2})}{r \Gamma(\beta/2)} - {}_2F_1\left(-\frac{1}{2}, \frac{\beta}{2}, \frac{3}{2}, -\frac{1}{\beta}r^2\right) \right\} - 2(r^2 + \beta) \right]. \quad (72)$$

Once again, in the limit $r \rightarrow \infty$, this quantity goes to zero,

while in the limit $r \rightarrow 0$ it can be expanded as

$$\bar{g}_{rr}(r, \beta) \approx \frac{\sqrt{\pi\beta} \Gamma(\frac{\beta-1}{2})}{16\Gamma(\beta/2) r} - \frac{1}{4} + \frac{3\sqrt{\pi}\Gamma(\frac{\beta-1}{2})}{16\sqrt{\beta}\Gamma(\frac{\beta}{2}-1)} r + \frac{\beta-3}{6\beta} r^2 + O(r^3). \quad (73)$$

This shows that the FS diverges in the limit $r \rightarrow 0$ as $1/r$ for any generic value of the Dyson index $\beta > 1$. We also note here the expression for \bar{g}_{rr} for $\beta = 3$ and $\beta = 5$, which take the following particularly simple forms

$$\bar{g}_{rr}(r, \beta = 3) = \frac{1}{8} \left(\frac{3 + 2r^2}{r\sqrt{3 + r^2}} - 2 \right). \quad (74)$$

and

$$\bar{g}_{rr}(r, \beta = 5) = \frac{1}{10r} \left(5\sqrt{5 + r^2} + r(4r(\sqrt{5 + r^2} - r) - 15) \right). \quad (75)$$

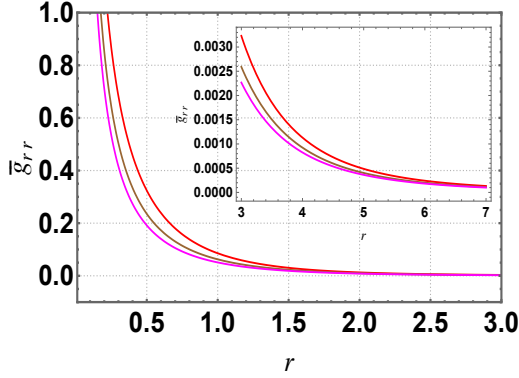


FIG. 7. Plot of $\bar{g}_{rr}(r, \beta)$ for a 2×2 ‘tridiagonal’ representation of the β ensemble for different values of the Dyson index, $\beta = 2$ (red), $\beta = 3$ (brown), and $\beta = 5$ (magenta). The plot in the inset shows more clearly the behaviour for large values of r .

In Fig. 7 we have shown the variation of $\bar{g}_{rr}(r, \beta)$ for these values of the Dyson index, along with the expression for $\beta = 2$. As can be seen, for higher values of β , $\bar{g}_{rr}(r, \beta)$ decays faster for large r , and its general behaviour is quite similar to the case of 2×2 rotationally invariant effective β ensemble studied next in section VII (see the plots in Figs. 9 and 10).

B. QMT for the tridiagonal β -ensemble

So far in this section, we have considered the simplest situation where the total Hamiltonian contains one parameter and the matrices are two-dimensional. Here we now consider the more general situation where the total Hamiltonian is assumed to be of the form (54), where the $N \times N$ matrices \mathcal{H}_i are now sampled from tridiagonal β -ensembles with generic Dyson indices. In Fig. 8 we have plotted the numerical values of the metric components for different fixed values of r (and with a fixed ϕ), when the matrix H_0 is drawn from a β -ensemble with a Dyson index $\gamma < 1$, and \mathcal{H}_1 and \mathcal{H}_2 are drawn from β -ensemble with the same Dyson index $\beta > 1$. Note that, compared with the previous cases of GUE Hamiltonians, the mixed component $g_{r\phi}$ is non-zero, and the numerical values of this component are shown in the inset of Fig. 8.

From this plot, we see that the overall behaviour of the three components is quite similar to each other, even though they approach zero for large r differently. Note that all the metric components diverge in the $r \rightarrow 0$ limit.

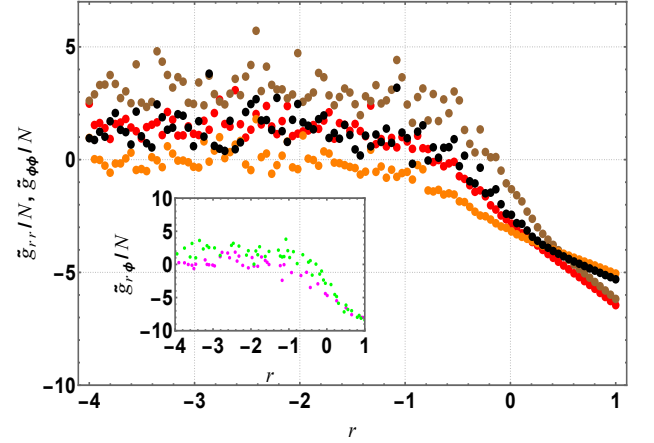


FIG. 8. Log-Log (with base 10) plot of the components of the metric tensor for Gaussian β -ensemble with large N . The Hamiltonian is of the same form as (54), with the individual matrices being drawn from β -ensemble with different Dyson indices (H_0 is from ensemble with Dyson index $\gamma < 1$, while \mathcal{H}_1 and \mathcal{H}_2 are drawn from β -ensemble with the same Dyson index $\beta > 1$). The red and the orange dots show the numerical values of the g_{rr} and $g_{\phi\phi}$ components, respectively, for fixed values of r and with $\beta = 2$ and $\gamma = 0.5$, while the brown and black dots represent these components when $\beta = 3$ and $\gamma = 0.2$. The plot in the inset shows the values of the $g_{r\phi}$ component for these two cases (magenta: $\beta = 2$ and $\gamma = 0.5$, and green: $\beta = 3$ and $\gamma = 0.2$). For all the plots, we have fixed $N = 1000$, and the results show expressions averaged over 1000 different realisations of the ensemble.

VII. THE FIDELITY-SUSCEPTIBILITY FOR AN INVARIANT β -ENSEMBLE WITH AN EFFECTIVE DYSON INDEX

In the previous section we have obtained the FS associated with a 2×2 random matrix ensemble with general Dyson index, by sampling the matrix from the tridiagonal matrix ensemble. However, as discussed, in this representation of the Gaussian β -ensemble, the ensemble with tridiagonal form is no longer invariant under symmetry transformations (unlike the classical Gaussian ensembles). In this section, we obtain the FS from a one-parameter family of 2×2 random matrix ensembles introduced in [71], which is rotationally invariant but has an effective real value of the Dyson index (β_e). As we have shown in the following, when a matrix drawn from this ensemble is added to a diagonal integrable Hamiltonian, the resulting FS ones again diverges as one moves to the integrable phase, suggesting that this feature is generic for random matrix ensembles having an integrability-to-chaos transition, irrespective of whether the underlying ensemble is rotational invariant or not.

A. A 2×2 matrix ensemble with an effective Dyson index

Consider the four random variables u, v, x, y taken from a one-parameter (η) dependent joint probability distribution $\mathbb{P}_\eta(u, v, x, y)$ and an ensemble defined by the following Hermi-

tion and unitary invariant 2×2 matrices,

$$\mathcal{H} = \begin{pmatrix} u & \frac{1}{\sqrt{2}}(x + iy) \\ \frac{1}{\sqrt{2}}(x - iy) & v \end{pmatrix} = \begin{pmatrix} u & se^{i\varphi} \\ se^{-i\varphi} & v \end{pmatrix}. \quad (76)$$

The expression for the joint probability distribution $\mathbb{P}_\eta(u, v, x, y)$ is given by [71]

$$\mathbb{P}_\eta(u, v, x, y) = Z_\eta e^{-\frac{1}{2}\text{Tr}\mathcal{H}^2} (2\text{Tr}\mathcal{H}^2 - (\text{Tr}\mathcal{H})^2)^{-\eta}, \quad (77)$$

where $\eta \in [0, 1]$, and Z_η is a normalisation constant. The resulting expression for the JPD of the eigenvalues (λ_1, λ_2) of the Hamiltonian \mathcal{H} is given by

$$P_\eta(\lambda_1, \lambda_2) = \mathcal{N}_\eta e^{-\frac{1}{2}(\lambda_1^2 + \lambda_2^2)} |\lambda_1 - \lambda_2|^{2-2\eta}, \quad (78)$$

where the normalisation constant is $\mathcal{N}_\eta = (\sqrt{\pi} 2^{3-2\eta} \Gamma(3/2 - \eta))^{-1}$. As can be seen, by making a comparison with the general expression for the JPD of eigenvalues in (6), $P_\eta(\lambda_1, \lambda_2)$ represents the JPD of eigenvalues of a 2×2 Gaussian β -ensemble with an effective Dyson index, $\beta_e = 2 - 2\eta \in [0, 2]$.¹⁶

When $\eta = 0$, the JPD of the matrix elements $\mathbb{P}_\eta(u, v, x, y)$ factorises (see eq. (77)), and the ensemble is reduced to the GUE with a strong correlation between the eigenvalues.

While on the other limit of the range, when $\eta = 1$, as can be seen from eq. (78), the JPD of the eigenvalues factorises, while matrix elements themselves are strongly correlated [71]. In the next section, we use these 2×2 matrix ensembles for different values of η to compute the FS.

B. Fidelity susceptibility for 2×2 invariant β -ensemble

We now use the 2×2 matrix ensemble with an effective Dyson index to discuss the geometry of eigenstates when a matrix belonging to this ensemble is added to an integrable Hamiltonian. Specifically, the total Hamiltonian once again takes the form (1), where the integrable term H_0 is taken to be of the form

$$H_0 = \begin{pmatrix} h_1 & 0 \\ 0 & h_2 \end{pmatrix}, \quad (79)$$

where h_1 and h_2 are two independently distributed Gaussian variables with the same mean and variance, and \mathcal{H} is drawn from a 2×2 invariant matrix ensemble with a generic Dyson index.

The expression for g_{rr} averaged over the ensemble can be written as

$$\tilde{g}_{rr}(r) = \frac{1}{Z(\eta)} \int \frac{\mathcal{H}_{12}\mathcal{H}_{21}}{(E_n - E_m)^2} (2\text{Tr}\mathcal{H}^2 - (\text{Tr}\mathcal{H})^2)^{-\eta} \exp\left[-\frac{1}{2}\text{Tr}(H_0^2 + \mathcal{H}^2)\right] dH_0 d\mathcal{H}, \quad (80)$$

where, the normalisation constant Z is given by the expression

$$Z(\eta) = \int \exp\left[-\frac{1}{2}\text{Tr}(H_0^2 + \mathcal{H}^2)\right] (2\text{Tr}\mathcal{H}^2 - (\text{Tr}\mathcal{H})^2)^{-\eta} dH_0 d\mathcal{H}. \quad (81)$$

Now using the matrix representations of \mathcal{H} and H_0 from eqs. (76) and (79), we get the following expression for $\tilde{g}_{rr}(r)$,

$$\begin{aligned} \tilde{g}_{rr}(r) &= \frac{1}{Z(\eta)} \int \frac{s^2 x_2^2}{(4s^2 r^2 + (x_2 + ry_2)^2)(4s^2 + y_2^2)^\eta} \exp\left[-\frac{1}{4}(4s^2 + x_1^2 + x_2^2 + y_1^2 + y_2^2)\right] ds dx_1 dx_2 dy_1 dy_2 \\ &= \frac{1}{Z(\eta)} \int \frac{s^2 x_2^2}{(4s^2 r^2 + (x_2 + ry_2)^2)(4s^2 + y_2^2)^\eta} \exp\left[-\frac{1}{4}(4s^2 + x_2^2 + y_2^2)\right] ds dx_2 dy_2. \end{aligned} \quad (82)$$

Here we have defined new coordinates, $h_{1,2} = (x_1 \pm x_2)/2$, $u = (y_1 + y_2)/2$ and $v = (y_1 - y_2)/2$. For $\eta = 0$, one gets back the expression for the GUE case considered in section V.

It seems difficult to obtain an analytical expression for $\tilde{g}_{rr}(r)$ by performing all the above integrals for generic values

η . Therefore, we evaluate it numerically for different fixed values of η . In Figs. 9 and 10 we have shown results of such numerical integration for $\eta = 1$ (i.e., $\beta_e = 0$) and $\eta = 1/2$ (corresponding to $\beta_e = 1$), respectively. We see that, for both cases, as expected, close to $r = 0$ the metric component diverges, while in the limit $r \rightarrow \infty$ it goes to zero. This behaviour is quite analogous to the rr component of the line element in (55). This is expected, since, if one directly considers the Hamiltonian $H = H_0 + r\mathcal{H}$, and computes the rr component assuming \mathcal{H} is a matrix belonging to the GUE, then this

¹⁶ It is important to note that the distribution in eq. (78) is not exactly that of Gaussian β -ensemble with $N = 2$, since β_e can take the value zero (for $\eta = 1$) which is not included in the standard β Gaussian ensembles [71].

is the same as the present case with $\eta = 0$. For comparison, we have also plotted the rr component of the metric in (55) in both Fig. 9 and Fig. 10 (magenta curve). As can be seen, the large r behaviour for both $\eta = 1$ and $\eta = 1/2$ match quite well with the analytical expression in (55) (corresponding, in this section, to $\eta = 0$), however, they start to differ as r is decreased (even though in all the cases the metric component diverges as $r \rightarrow 0$).

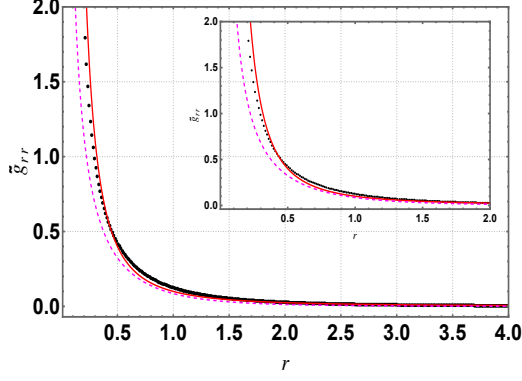


FIG. 9. Plot of $\tilde{g}_{rr}(r)$ for the effective β ensemble with $\eta = 1$, i.e., $\beta_e = 0$ (black dots). The red curve shows a simple inverse square fitting of the numerical data: $\tilde{g}_{rr}(r) \approx 0.1/r^2$. The magenta dot-dashed curve is the plot for the rr component of the line element for the GUE case (see eq. (55)). The plot in the inset shows more clearly the fitting for large values of r .

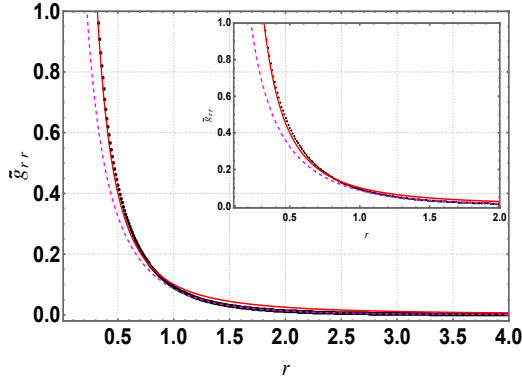


FIG. 10. Plot of $\tilde{g}_{rr}(r)$ for the effective β ensemble with $\eta = 1/2$, i.e., $\beta_e = 1$ (black dots). The red curve shows an inverse square fitting of the numerical data: $\tilde{g}_{rr}(r) \approx 0.1/r^2$. The magenta dot-dashed curve is the plot for the rr component of the line element for the GUE case (see eq. (55)). The plot in the inset shows more clearly the fitting for large values of r .

Comparing plots with $\eta = 1$ and $\eta = 1/2$, another possible conclusion one can draw is that, even though there is a $(E_m - E_n)^2$ term in the denominator of the definition of $\tilde{g}_{rr}(r)$, its decay with respect to r may not be due to the correlation and repulsion between the eigenvalues but rather due to the fact that this energy difference term increases with increasing r . Thus, as $r \rightarrow \infty$, $\tilde{g}_{rr}(r)$ goes to zero even for $\eta = 1$ - the case where there is no correlation between the eigenvalues of the

Hamiltonian of this invariant 2×2 β -ensemble.

VIII. CONCLUSIONS AND DISCUSSIONS

In this paper we have considered the geometry of the quantum states for random matrix Hamiltonians that belong to some specific ensembles. The random matrix universality in the energy eigenvalues is commonly taken as a signature of chaotic behaviour of many-body quantum systems in the sense that fine-grained properties of the energy spectrum of these complex quantum many-body systems are well approximated by the random matrix theory [23, 24]. Nevertheless, it is also important to understand the properties of the eigenstates of these many-body Hamiltonians, possibly, as a first approximation, by modelling them with random matrices. Instead of using the conventional tools for this purpose, such as the inverse partition ratio of these eigenstates in a complete basis, here we have used the natural geometry of the space of quantum states induced by the Hermitian inner product, which measures the infinitesimal distance between two states. Here we focus specifically on random matrix Hamiltonians, which are drawn from ensembles that are more general than those of the three classical Gaussian ensembles and show a chaos-to-integrability transition. In particular, we have focused our attention on two generalisations of the classical Gaussian ensembles, namely the RP random matrix ensemble and the tridiagonal Gaussian β -ensembles, both of which show chaos-to-integrability transition in the level spacing distribution of the energy eigenvalues and break the rotational invariance of the classical Gaussian ensembles.¹⁷ It is possible to obtain the (suitably averaged) QMT on the parameter space (in some cases analytically) and explore how it encodes different characteristic properties of the eigenstates of the random matrix Hamiltonian under consideration.

We now briefly summarise the important conclusions and lessons obtained in this paper.

1. In sections III and V, we have studied in detail different geometric quantities calculated from the QMTs corresponding to both a chaotic Hamiltonian (belonging to the GUE) and a Hamiltonian which shows a chaos-to-integrability transition. The Ricci scalar corresponding to this two-dimensional geometry changes from a constant to a non-constant value as the unitary symmetry of the GUE is broken. For the generalised RP model, the Ricci scalar shows a regular behaviour with parameter r which controls the ‘amount’ of unitary symmetry breaking, e.g., for a small value of r , when the system is close to an integrable phase, the Ricci scalar starts from a constant value at $r = 0$ (which is smaller than the constant value it takes for the GUE Hamiltonian) and gradually reaches the constant value taken deep within the chaotic phase.

The geodesics corresponding to the QMTs also reveal interesting information about the geometry of these parameter

¹⁷ We have also considered a specific form of the β -ensemble which keeps the invariance intact.

manifolds. We showed that starting from a point on the parameter manifold very close to the integrable phase, any arbitrary point deep in the chaotic phase (corresponding to a large value of the parameter r) can be reached for a finite value of the affine parameter that parametrises the geodesic paths.

2. In section IV, we have discussed the procedure of obtaining the FS (and the components of the QMT in general), from the connected correlation function involving the \mathcal{H} term in the total Hamiltonian $H = H_0 + r\mathcal{H}$. Specifically, we have shown that the SFF, which controls the time-dependent part of the above-mentioned correlation function, is related to the FS. In fact, the part of the SFF that comes from the two-point correlation function of the random matrix ensemble is directly responsible for the N -dependent part of the FS.

3. For a different class of random matrix ensembles with a general Dyson index, and which shows a chaos-to-integrability transition, we have obtained the FS and showed that it diverges as one moves close to the integrable point. This is true for either of the ensembles, one of which does not have rotational invariance (the tridiagonal Gaussian β -ensemble) and the other one has rotational invariance, as discussed in section VII (see also the computation of the FS in Appendix E for an ensemble having random eigenvectors and eigenvalues drawn from Gaussian β -ensemble).

We conclude by pointing out a few interesting future directions along which the results presented in this paper can be extended.

1. As we have seen in section V, the Ricci scalar of the averaged QMT takes a generic parameter-dependent expression compared to a fixed constant in the chaotic phase. Since the Ricci scalar being constant seems to be related to the fact that the GUE has rotational symmetry, it will be interesting to investigate whether the Ricci curvature scalar associated with the QMT for realistic quantum many-body systems showing an integrability-to-chaos transition shows similar behaviour.

2. In this paper, we mostly consider the Gaussian weight function, i.e., potentials of the form $V(H) = H^2$. However, one can consider more general weight functions, for which the ensemble would still retain the rotational invariance of the classical Gaussian ensembles (even though the individual elements of the Hamiltonian matrix will not be independent) and study the ensemble-averaged QMT and its related quantities for such ensembles.

3. Finally, in this work, we have assumed that the Hamiltonian governing the dynamics is Hermitian and consequently the ‘curvature’ of the parameter manifold is induced by the Hermitian inner product, which was reflected in the behaviour of the geometry in the integrability to chaotic transitions. However, this feature will no longer be true in the cases where the dynamics of the many-body systems are governed by the non-Hermitian Hamiltonian, and in fact, the state-space geometry will be far richer than the one considered here. Extending these results to the non-Hermitian cases, it would be interesting to investigate how the Ricci scalar of the QMT behaves under transitions between non-Hermitian integrable and chaotic regimes, in particular since, unlike the standard Hermitian case, the bi-orthogonal nature of the inner product induces a non-Hermitian tensor structure on the base manifold,

it would be interesting to study the curvature structure of such models.

Acknowledgments

It is a pleasure to thank Hugo A. Camargo, Yichao Fu, and Viktor Jahnke for many insightful discussions and for comments on a draft version of the manuscript. The work of Kunal Pal is supported by the YST Program at the APCTP through the Science and Technology Promotion Fund and Lottery Fund of the Korean Government. This was also supported by the Korean Local Governments - Gyeongsangbuk-do Province and Pohang City. This work was supported by the Basic Science Research Program through the National Research Foundation of Korea (NRF) funded by the Ministry of Science, ICT & Future Planning (NRF-2021R1A2C1006791, NRF-2020R111A2054376), the framework of international cooperation program managed by the NRF of Korea (RS-2023-NR119907, RS-2024-00440725), the Creation of the Quantum Information Science R&D Ecosystem (Grant No. 2022M3H3A106307411) through the NRF funded by the Korean government (Ministry of Science and ICT), the Gwangju Institute of Science and Technology (GIST) research fund (Future leading Specialized Research Project, 2025) and the AI-based GIST Research Scientist Project grant funded by the GIST in 2025.

Appendix A: QGT for a generic superposition of eigenstates

For completeness, here, we record the expression for the QGT

$$g_{ab}(\mathbf{r}) = \langle \partial_a \Psi(\mathbf{r}) | \partial_b \Psi(\mathbf{r}) \rangle - \langle \partial_a \Psi(\mathbf{r}) | \Psi(\mathbf{r}) \rangle \langle \Psi(\mathbf{r}) | \partial_b \Psi(\mathbf{r}) \rangle, \quad (\text{A1})$$

for a generic superposition of eigenstates, $|\Psi(\mathbf{r})\rangle = \sum_n c_n |n(\mathbf{r})\rangle$, where c_n s are complex numbers independent of the set of parameters $\{\mathbf{r}\}$ present in the total Hamiltonian. A straightforward calculation shows that the expression for the QGT can be written as

$$g_{ab}(\mathbf{r}) = \sum_{n,m} c_n^* c_m \left(\sum_k (1 - |c_k|^2) \langle \partial_a n(\mathbf{r}) | k(\mathbf{r}) \rangle \langle k(\mathbf{r}) | \partial_b m(\mathbf{r}) \rangle - \sum_{k \neq l} c_k c_l^* \langle \partial_a n(\mathbf{r}) | k(\mathbf{r}) \rangle \langle l(\mathbf{r}) | \partial_b m(\mathbf{r}) \rangle \right). \quad (\text{A2})$$

Specifically, for the state $|\Psi(\mathbf{r})\rangle = N^{-1/2} \sum_n |n(\mathbf{r})\rangle$, the components of QGT are given by

$$g_{ab}(\mathbf{r}) = \frac{1}{N} \sum_{n,m} \left(\sum_k (1 - \frac{1}{N}) \langle \partial_a n(\mathbf{r}) | k(\mathbf{r}) \rangle \langle k(\mathbf{r}) | \partial_b m(\mathbf{r}) \rangle - \sum_{k \neq l} \frac{1}{N} \langle \partial_a n(\mathbf{r}) | k(\mathbf{r}) \rangle \langle l(\mathbf{r}) | \partial_b m(\mathbf{r}) \rangle \right). \quad (\text{A3})$$

As can be seen, the last two expressions, in general, represent different quantities from that of the average QGT over all the eigenstates, i.e., eq. (19).

Appendix B: Derivation of QMT component for GUE Hamiltonian

In this Appendix, we briefly present the derivation of the rr component of the ensemble-averaged QMT (\bar{g}_{rr} in (24)) for the GUE Hamiltonian in (21).¹⁸ We start by writing the first expression in (22) explicitly (since $H = H_0 + r\tilde{H}_1$),

$$\bar{g}_{rr}(r) = \frac{1}{NZ} \sum_{m \neq n} \int \frac{(\tilde{H}_1)_{nm}(\tilde{H}_1)_{mn}}{(E_n(r) - E_m(r))^2} \times \exp \left[-\frac{1}{2\sigma^2} (\text{Tr}(H_0^2) + \text{Tr}(\tilde{H}_1^2)) \right] dH_0 d\tilde{H}_1, \quad (\text{B1})$$

where we have performed the trivial integration over \tilde{H}_2 . Now performing two successive variable changes: first using $H_0 = H - r\tilde{H}_1$ and subsequently $\tilde{H}_1 = \frac{H_1}{\sqrt{r^2+1}} + \frac{r}{r^2+1}H$, we can rewrite

$$\bar{g}_{rr}(r) = \frac{1}{NZ(r^2+1)} \sum_{m \neq n} \int \frac{(H_1)_{nm}(H_1)_{mn}}{(E_n(r) - E_m(r))^2} \times \exp \left[-\frac{1}{2\sigma^2} \left(\frac{\text{Tr}(H^2)}{r^2+1} + \text{Tr}(H_1^2) \right) \right] dH dH_1. \quad (\text{B2})$$

Note that the motivation behind these particular coordinate changes is to write the total probability distribution in a form which factorises in two variables, one of which should be the total Hamiltonian H . Also note that, with the conventions fixed at the beginning of section III, the variance of the vari-

the above expression as,¹⁹

able H_1 is σ^2 . We can perform the integral over H_1 by using the standard formula for the correlator of the GUE matrices, $\mathbb{E}((H_1)_{ij}(H_1)_{kl}) = \sigma^2 \delta_{il} \delta_{jk}$. Since we have fixed $\sigma^2 = 1/N$, we then have,

$$\bar{g}_{rr}(r) = \frac{1}{N^2 Z(r^2+1)} \sum_{m \neq n} \int \frac{1}{(E_n(r) - E_m(r))^2} \exp \left[-\frac{1}{2\sigma^2} \left(\frac{\text{Tr}(H^2)}{r^2+1} \right) \right] dH = \frac{1}{N^2(r^2+1)} \sum_{m \neq n} \mathbb{E} \left[\frac{1}{(E_n(r) - E_m(r))^2} \right]_{\text{GUE}(\sigma_\star^2)}, \quad (\text{B3})$$

where $\sigma_\star^2 = \sigma^2(r^2+1)$. The expression in the final step above can be evaluated using a result obtained by Dyson [72], known as the virial theorem associated with the Brownian motion approach to the eigenvalue distribution of a Gaussian random matrix. For a classical Gaussian random matrix ensemble with a Dyson index $\beta > 1$, and variance σ_\star^2 , the virial theorem states [72],

$$\sum_{m \neq n} \mathbb{E} \left[\frac{1}{(E_n - E_m)^2} \right]_{\text{GUE}(\sigma_\star^2)} = \frac{N(N-1)}{2\sigma_\star^2 \beta (1 - \beta^{-1})}. \quad (\text{B4})$$

Now using this relation, along with the fact that here $\sigma_\star^2 = \frac{r^2+1}{N}$, we get the required expression

$$\bar{g}_{rr}(r) = \frac{N-1}{2(r^2+1)^2}. \quad (\text{B5})$$

By following a similar analysis, one can obtain the other components of the metric tensor in (24).

Appendix C: Coordinate transformations to the metric of S^2

Here, we briefly discuss the coordinate transformation, which maps the line element into the round metric on the 2-sphere S^2 . Taking $r^2 = \cot^2 \theta$, with $\theta \in [-\pi/2, \pi/2]$, we get the transformed line element (with $A = (N-1)/2$)

$$ds^2 = A(d\theta^2 + \cos^2 \theta d\phi^2). \quad (\text{C1})$$

¹⁸ We note that the derivation presented in [42] contains a few typographical errors.

¹⁹ All the Jacobian factors associated with these transformations are constant, and hence cancel from the same factors form the integral in Z in the denominator.

This is essentially the round metric on the two-dimensional sphere. For convenience, here we also provide the first-order geodesic equations, which in the (θ, ϕ) coordinates are given by

$$L = A \sin^2 \theta(\lambda) \dot{\phi}(\lambda), \quad \dot{\theta}^2(\lambda) = \frac{1}{A^2} (K A - L^2 \operatorname{cosec}^2 \theta(\lambda)). \quad (\text{C2})$$

If we consider any two points on the sphere (say, $P_1(\theta_0, \phi_0)$ and $P_2(\theta_1, \phi_1)$), then these can always be connected by a great circle. The geodesic connecting P_1 and P_2 is the two segments of this great circle. The geodesic distance between them is given by the following well-known expression,

$$L = \arccos \left[\sin \left(\frac{\theta_0}{\sqrt{A}} \right) \sin \left(\frac{\theta_1}{\sqrt{A}} \right) + \cos \left(\frac{\theta_0}{\sqrt{A}} \right) \cos \left(\frac{\theta_1}{\sqrt{A}} \right) \cos(\phi_0 - \phi_1) \right]. \quad (\text{C3})$$

Appendix D: Alternative expression for the correlation function with GUE matrix

In this section, we discuss an alternative expression for the correlation function in eq. (36) that will illustrate some important points regarding how these correlation functions evolve with time and the role of the rank of the Hamiltonian N , specifically the limit $N \rightarrow \infty$.

To compute the required correlation function, in the following, we follow an approach inspired by the free probability theory [47, 48, 73]. The basic idea is the following. Since the random matrices H_0 and V are independent, in the limit of large $N \rightarrow \infty$, they become free random variables. However, since in the correlation function the time evolution is generated by the total Hamiltonian \tilde{H} , what we need is a random variable which is free from \tilde{H} . One way of doing this is to find out an orthogonal transformation which transforms the free variables H_0 and V to the new free variables \tilde{H} and, say, X . After obtaining X in terms of H_0 and V , one can transform moments of the form $\langle \tilde{H} V(t) \tilde{H} V \rangle$ into moments in terms of mutually free variables, as, $\langle \tilde{H} X(t) \tilde{H} X \rangle$, which can then be computed using free probability.²⁰

It can be checked that the required orthogonal transformation is the following,

$$\begin{pmatrix} X \\ \tilde{H} \end{pmatrix} = \frac{1}{\alpha} \begin{pmatrix} \sigma & -r\sigma \\ r\sigma & \sigma \end{pmatrix} \begin{pmatrix} \tilde{V} \\ \tilde{H}_0 \end{pmatrix}, \quad (\text{D1})$$

where $\alpha = \sqrt{(r^2 + 1)\sigma}$. Note that the expression for the random matrix X is the same as the one obtained in (39) by requiring that the total probability distribution factorises in terms of the variables \tilde{H} and X - another way of getting independent Gaussian variables. Since X and H are independent variables, drawn from Gaussian ensembles, in the limit $N \rightarrow \infty$, they

would be free variables. Now we can rewrite the correlator $\langle V(t)V \rangle$ under consideration as follows

$$\begin{aligned} \langle V(t)V \rangle &= r^2 \sigma^2 \langle \tilde{V}(t) \tilde{V} \rangle \\ &= \frac{r^2 \sigma^2}{\alpha^2} \langle e^{i\tilde{H}t} (\sigma X + r\sigma \tilde{H}) e^{-i\tilde{H}t} (\sigma X + r\sigma \tilde{H}) \rangle \\ &= \frac{r^2 \sigma^2}{\alpha^2} (\sigma^2 \langle X(t)X \rangle + 2r\sigma^2 \langle X\tilde{H} \rangle + r^2 \sigma^2 \langle \tilde{H}^2 \rangle). \end{aligned} \quad (\text{D2})$$

Using the fact that $\langle X \rangle = \langle \tilde{H} \rangle = 0$, we see that $\langle X\tilde{H} \rangle = 0$ from the freeness of these two variables. Furthermore, the correlator $\langle X(t)X \rangle$ can be expanded in a Taylor series with terms of the form $\langle \tilde{H}^i X \tilde{H}^j X \rangle$. Once again, using the property of free variables that the crossing partitions do not contribute in the moment expansion, these moments can be evaluated by noting that the only diagram that has a non-zero contribution gives a result of the form $\langle \tilde{H}^i \rangle \langle X^2 \rangle \langle \tilde{H}^j \rangle$. Using all these inputs in eq. (D2) we get the final form of the desired correlator to be (using $\langle X^2 \rangle = N$)

$$\begin{aligned} \langle V(t)V \rangle &= \frac{r^2 \sigma^2}{\alpha^2} (\sigma^2 \langle X^2 \rangle |\langle e^{-i\tilde{H}t} \rangle|^2 + r^2 \sigma^2 N) \\ &= \frac{r^2 N \sigma^2}{r^2 + 1} (|\langle e^{-i\tilde{H}t} \rangle|^2 + r^2). \end{aligned} \quad (\text{D3})$$

Now noting that the average density of states of the Hamiltonian \tilde{H} is $\tilde{\rho}(\lambda) = \sqrt{4N - \lambda^2}/(2\pi N)$ when $\sigma = 1/\sqrt{N}$, we can write the above correlator as

$$\langle V(t)V \rangle = r^2 \langle \mathcal{H}(t)\mathcal{H} \rangle = \frac{r^2}{(r^2 + 1)} \left(({}_0F_1(2, -Nt^2))^2 + r^2 \right), \quad (\text{D4})$$

where ${}_0F_1(b, x)$ denotes the regularized Hypergeometric function. We remind that, since we have used the freeness between two large Gaussian variables, the expression for the correlator in is also valid strictly in the large $N \rightarrow \infty$ limit. For finite values of N , the expression derived in (42) gives a more accurate expression. See Fig. 1 for a comparison of the two analytical expressions (one derived here and the one in (42)) with the numerical result.

Comparing this expression for the correlator (in (D4)) with the earlier expression derived in (42), we see that, in this expression, the time dependence comes from only the connected part of the SFF, whereas, in (42), the full SFF contributes to the correlation function. This is essentially related to the fact that in the large N limit all the terms in the SFF, apart from the one coming the disconnected part of the two-point density correlation function vanish in the $N \rightarrow \infty$ limit.

To see this explicitly, consider the correlation function obtained in (43) for the non-scaled Hamiltonian. By using the so-called box approximation [58–60], one obtains the following approximate expression for the SFF for a GUE Hamiltonian,

$$\mathcal{R}(t') = N + N^2 |\langle e^{-it'H'} \rangle|^2 - N r_2(t'), \quad (\text{D5})$$

where

$$|\langle e^{-it'H'} \rangle|^2 = \left(\frac{J_1(2t')}{t'} \right)^2, \quad \text{and} \quad r_2(t') = \begin{cases} 1 - \frac{t'}{2N}, & \text{for } t' < 2N \\ 0, & \text{for } t' > 2N. \end{cases} \quad (\text{D6})$$

²⁰ In the following we follow an approach outlined in [74].

Here $|\langle e^{-it'H'} \rangle|^2$ denotes the contribution of the disconnected piece of the 2-point correlation function, while $r_2(t')$ is the contribution of the connected part that gives rise to the ramp in the SFF. Now, due to the N^2 factor present in the denominator of (43), we see from the above expression for $\mathcal{R}(t')$ that both the constant term and the contribution coming from the connected part ($r_2(t')$) are suppressed as $1/N$ in the limit $N \rightarrow \infty$, and the only contribution in this limit comes from $|\langle e^{-it'H'} \rangle|^2$. Note that the function $r_2(t')$ is only non-zero up to a timescale $t' < 2N$, hence even though this term is linearly increasing, in the late times $t' > 2N$ it does not contribute to the correlation function. In the free probabilistic computation, in eq. (D2), this can be traced back to the fact that only non-crossing partitions contribute to the moments [75].

Appendix E: Computation of the fidelity susceptibility for a 2×2 random matrix ensemble

In this Appendix, we present a random matrix ensemble with generic Dyson index β , which we use to compute the FS, both for the case of ensembles with only chaotic phase, and also one showing a chaos-to-integrability transition.

We consider the following two 2×2 diagonal matrices with

$$\bar{g}_{rr}(r) = \frac{1}{Z} \int \frac{h_{12}^2 v_{12}^2 \cos^2 \theta \sin \theta^2}{(h_{12}^2 + v_{12}^2 r^2 + 2rh_{12}v_{12} \cos 2\theta)^2} \times P(h_1, h_2) P(v_1, v_2) dh_1 dh_2 dv_1 dv_2 \sin 2\theta d\theta. \quad (\text{E4})$$

Here, $P(h_1, h_2)$ and $P(v_1, v_2)$ are the joint probability distribution of the eigenvalues in eq. (6) having a general value of the Dyson index β . We assume that both matrices are drawn from ensembles with the same Dyson index. Performing coordinate transformations $h_1 - h_2 = \varrho \sin \varphi$ and $v_1 - v_2 = \varrho \cos \varphi$, we see that all the integrals, except the one over φ , can be performed analytically. Finally, evaluating the resulting integral over φ numerically, we plot the results for different values of β in Fig. 11. For $\beta = 2$, the result matches exactly with the GUE expression in eq. (24) with $N = 2$. Changing values of the Dyson index, we see that decreasing the value of β , the FS keeps increasing for small values of r , and in the limit $\beta \rightarrow 0$ the FS diverges as $r \rightarrow 0$. This conclusion is consistent with the ones in section VI.

real entries

$$H_0 = \begin{pmatrix} h_1 & 0 \\ 0 & h_2 \end{pmatrix}, \quad V = \begin{pmatrix} v_1 & 0 \\ 0 & v_2 \end{pmatrix}, \quad (\text{E1})$$

and consider rotating one of them by a random unitary matrix sampled from the Haar unitary group,

$$U = \begin{pmatrix} e^{iu_1} \cos \theta & -e^{iu_2} \cos \theta \\ e^{-iu_2} \cos \theta & e^{-iu_1} \cos \theta \end{pmatrix}. \quad (\text{E2})$$

In the following, we assume that the joint eigenvalues of the matrices H_0 and V are independent, and are drawn from the joint probability distribution (6) of the Gaussian β -ensemble. The total Hamiltonian of the system we consider is given by

$$H(r) = H_0 + r UVU^\dagger. \quad (\text{E3})$$

In this representation, therefore, the total Hamiltonian $H(r)$ and the term $\mathcal{H} = UVU^\dagger$ are written, without loss of generality, in terms of the eigenbasis of the matrix H_0 . We performed a random rotation of the matrix V to make its eigenvectors generic with respect to those of H_0 . Note that the total Hamiltonian can be decomposed into two parts, one of which is proportional to the identity matrix, and a generic non-diagonal part which depends on the parameters of the unitary matrix U .

Case 1. First, consider the case where the joint probability distributions of both h_i and v_i are the same, i.e., the ensembles from which these matrices are drawn have the same Dyson index. The ensemble-averaged FS computed from this Hamiltonian is given by (with $h_{12} = h_1 - h_2$ and $v_{12} = v_1 - v_2$)

Case 2. Next, we consider the situation where the joint probability distributions of h_i and v_i are different, in particular, we assume that the eigenvalues of the matrix H_0 are drawn from independent Gaussian distributions with mean zero and unit variance, while the JPD of eigenvalues of V ($P(v_1, v_2)$) follows that of Gaussian β -ensemble with generic β . Once again, by performing coordinate transformations $h_1 - h_2 = \varrho \sin \varphi$ and $v_1 - v_2 = \varrho \cos \varphi$, one can perform all the integrals appearing in $\bar{g}_{rr}(r)$, apart from the one over φ , which can easily be done numerically. The resulting FS is shown in Fig. 12. When the $\beta = 2$, the result matches with the expression in (55). Furthermore, as in the case of ensembles discussed in sections VI and VII, the FS diverges in the limit $r \rightarrow 0$, i.e., as the Hamiltonian goes to the integrable phase.

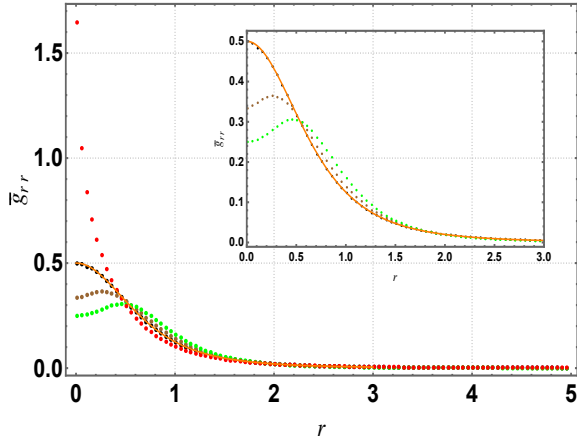


FIG. 11. Plot of $\bar{g}_{rr}(r)$ for a 2×2 Hamiltonian of the form $H(r) = H_0 + r UVU^\dagger$, where eigenvalues of both the matrices H_0 and V have correlations, and are drawn from joint probability distribution of the Gaussian β -ensemble. We have shown the results when eigenvalues of both these matrices follow JPD in (6) with the same Dyson index, and for several different cases, $\beta = 1$ (red dots), $\beta = 2$ (black), $\beta = 3$ (brown), and $\beta = 5$ (green). The solid orange curve shows the exact GUE expression in eq. (24) with $N = 2$. As the value of the Dyson index is decreased, and gradually the limit $\beta \rightarrow 0$ limit is approached, the $\bar{g}_{rr}(r)$ diverges when $r \rightarrow 0$. The plot in the inset shows more clearly the behaviour for large values of $\beta \geq 2$.

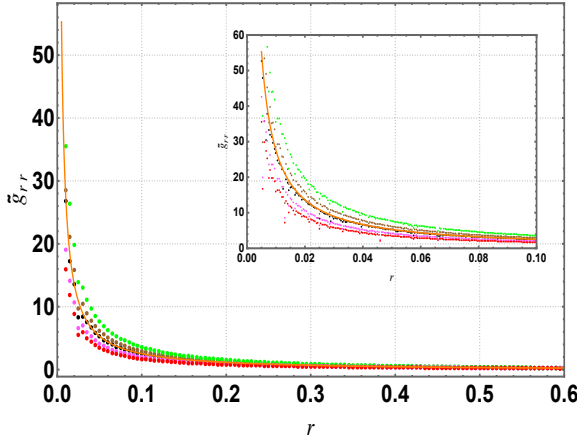


FIG. 12. Plot of $\bar{g}_{rr}(r)$ for a 2×2 Hamiltonian of the form $H(r) = H_0 + r UVU^\dagger$, where eigenvalues of the matrices H_0 are drawn from independent Gaussian distributions, while those of V have correlations, and are drawn from joint probability distribution of the Gaussian β -ensemble. We have shown the results for different values of the Dyson index, $\beta = 1$ (red dots), $\beta = 2$ (black), $\beta = 3$ (brown), and $\beta = 5$ (green). The solid orange curve shows the exact expression in eq. (55), which matches exactly with the $\beta = 2$ case numerically obtained from this ensemble. The plot in the inset shows more clearly the behaviour for small values of r , where the FS diverges in the limit $r \rightarrow 0$.

[2] D. Chruściński and A. Jamiolkowski, *Geometric phases in classical and quantum mechanics* (Springer, 2004).
 [3] T. W. Kibble, *Communications in Mathematical Physics* **65**, 189 (1979).

[4] A. Ashtekar and T. A. Schilling, arXiv e-prints gr-qc/9706069 (1997), gr-qc/9706069.
 [5] D. C. Brody and L. P. Hughston, *Journal of Geometry and Physics* **38**, 19 (2001), quant-ph/9906086.
 [6] J. Provost and G. Vallee, *Communications in Mathematical Physics* **76**, 289 (1980).
 [7] M. V. Berry, *Proceedings of the Royal Society of London. A. Mathematical and Physical Sciences* **392**, 45 (1984).
 [8] B. Simon, *Phys. Rev. Lett.* **51**, 2167 (1983), URL <https://link.aps.org/doi/10.1103/PhysRevLett.51.2167>.
 [9] P. Zanardi, P. Giorda, and M. Cozzini, *Phys. Rev. Lett.* **99**, 100603 (2007).
 [10] W.-L. You, Y.-W. Li, and S.-J. Gu, *Phys. Rev. E* **76**, 022101 (2007), URL <https://link.aps.org/doi/10.1103/PhysRevE.76.022101>.
 [11] L. C. Venuti and P. Zanardi, *Physical Review Letters* **99**, 095701 (2007).
 [12] M. Kolodrubetz, V. Gritsev, and A. Polkovnikov, *Phys. Rev. B* **88**, 064304 (2013), URL <https://link.aps.org/doi/10.1103/PhysRevB.88.064304>.
 [13] P. Kumar and T. Sarkar, *Phys. Rev. E* **90**, 042145 (2014), URL <https://link.aps.org/doi/10.1103/PhysRevE.90.042145>.
 [14] A. Dey, S. Mahapatra, P. Roy, and T. Sarkar, *Phys. Rev. E* **86**, 031137 (2012), URL <https://link.aps.org/doi/10.1103/PhysRevE.86.031137>.
 [15] L. Henriot, *Phys. Rev. B* **97**, 195138 (2018), URL <https://link.aps.org/doi/10.1103/PhysRevB.97.195138>.
 [16] D. Gutiérrez-Ruiz, J. Chávez-Carlos, D. Gonzalez, J. G. Hirsch, and J. D. Vergara, *Phys. Rev. B* **105**, 214106 (2022), URL <https://link.aps.org/doi/10.1103/PhysRevB.105.214106>.
 [17] J. Štřeleček and P. Cejnar, *Phys. Rev. A* **111**, 012211 (2025), URL <https://link.aps.org/doi/10.1103/PhysRevA.111.012211>.
 [18] A. Alexandrov and A. Gorsky, *Phys. Rev. E* **107**, 044211 (2023), URL <https://link.aps.org/doi/10.1103/PhysRevE.107.044211>.
 [19] D. Xiao, M.-C. Chang, and Q. Niu, *Rev. Mod. Phys.* **82**, 1959 (2010), URL <https://link.aps.org/doi/10.1103/RevModPhys.82.1959>.
 [20] T. Ozawa and B. Mera, *Phys. Rev. B* **104**, 045103 (2021), URL <https://link.aps.org/doi/10.1103/PhysRevB.104.045103>.
 [21] B. Mera and T. Ozawa, *Phys. Rev. B* **104**, 045104 (2021), URL <https://link.aps.org/doi/10.1103/PhysRevB.104.045104>.
 [22] F. J. Dyson, *Journal of Mathematical Physics* **3**, 1199 (1962).
 [23] O. Bohigas, M.-J. Giannoni, and C. Schmit, *Physical review letters* **52**, 1 (1984).
 [24] M. V. Berry, *Proceedings of the Royal Society of London. A. Mathematical and Physical Sciences* **400**, 229 (1985).
 [25] E. Bogomolny, U. Gerland, and C. Schmit, *Physical Review E* **59**, R1315 (1999).
 [26] M. Robnik, *Mathematics and Computers in Simulation* **40**, 159 (1996).
 [27] T. Cheon, T. Mizusaki, T. Shigehara, and N. Yoshinaga, *Physical Review A* **44**, R809 (1991).
 [28] A. Csordás, R. Graham, P. Szépfalusy, and G. Vattay, *Physical Review E* **49**, 325 (1994).
 [29] G. Lenz and F. Haake, *Physical review letters* **67**, 1 (1991).
 [30] P. Shukla and A. Pandey, *Nonlinearity* **10**, 979 (1997).
 [31] M. Potters and J.-P. Bouchaud, *A First Course in Random Matrix Theory* (Cambridge University Press, 2020).

- [32] M. Mehta, *Random Matrices* (Academic Press, 1991), URL <https://books.google.co.kr/books?id=vBHSAQAACAAJ>.
- [33] N. Rosenzweig and C. E. Porter, *Physical Review* **120**, 1698 (1960).
- [34] V. Kravtsov, I. Khaymovich, E. Cuevas, and M. Amini, *New Journal of Physics* **17**, 122002 (2015).
- [35] T. Čadež, D. K. Nandy, D. Rosa, A. Andreanov, and B. Dietz, *New Journal of Physics* **26**, 083018 (2024).
- [36] W. Buijsman, *Phys. Rev. B* **109**, 024205 (2024), URL <https://link.aps.org/doi/10.1103/PhysRevB.109.024205>.
- [37] G. De Tomasi and I. M. Khaymovich, *Phys. Rev. B* **106**, 094204 (2022), URL <https://link.aps.org/doi/10.1103/PhysRevB.106.094204>.
- [38] P. von Soosten and S. Warzel, *Letters in Mathematical Physics* **109**, 905 (2019).
- [39] D. Facoetti, P. Vivo, and G. Biroli, arXiv preprint arXiv:1607.05942 (2016).
- [40] I. Dumitriu and A. Edelman, *Journal of Mathematical Physics* **43**, 5830 (2002), ISSN 0022-2488, URL <https://doi.org/10.1063/1.1507823>.
- [41] W. Buijsman, V. Cheianov, and V. Gritsev, *Physical review letters* **122**, 180601 (2019).
- [42] R. Sharipov, A. Tiutiakina, A. Gorsky, V. Gritsev, and A. Polkovnikov (2024), 2411.11968.
- [43] P. Hauke, M. Heyl, L. Tagliacozzo, and P. Zoller, *Nature Physics* **12**, 778 (2016).
- [44] M. Kolodrubetz, D. Sels, P. Mehta, and A. Polkovnikov, *Physics Reports* **697**, 1 (2017).
- [45] W.-L. You and L. He, *Journal of Physics: Condensed Matter* **27**, 205601 (2015).
- [46] E. Brézin and S. Hikami, *Phys. Rev. E* **55**, 4067 (1997), URL <https://link.aps.org/doi/10.1103/PhysRevE.55.4067>.
- [47] D. V. Voiculescu, K. J. Dykema, and A. Nica, *Free random variables*, vol. 1 (American Mathematical Soc., 1992).
- [48] J. A. Mingo and R. Speicher, *Free probability and random matrices*, vol. 35 (Springer, 2017).
- [49] A.-G. Penner, F. von Oppen, G. Zarand, and M. R. Zirnbauer, *Phys. Rev. Lett.* **126**, 200604 (2021), 2011.03557.
- [50] P. N. Walker and M. Wilkinson, *Phys. Rev. Lett.* **74**, 4055 (1995), URL <https://link.aps.org/doi/10.1103/PhysRevLett.74.4055>.
- [51] M. Berry and P. Shukla, *Journal of Physics A: Mathematical and Theoretical* **53**, 275202 (2020).
- [52] S. M. Carroll, *Spacetime and geometry* (Cambridge University Press, 2019).
- [53] H. J. Lipkin, N. Meshkov, and A. J. Glick, *Nucl. Phys.* **62**, 188 (1965).
- [54] N. Meshkov, A. J. Glick, and H. J. Lipkin, *Nucl. Phys.* **62**, 199 (1965).
- [55] A. J. Glick, H. J. Lipkin, and N. Meshkov, *Nucl. Phys.* **62**, 211 (1965).
- [56] K. Pal, K. Pal, and T. Sarkar, *Phys. Rev. E* **107**, 044130 (2023), URL <https://link.aps.org/doi/10.1103/PhysRevE.107.044130>.
- [57] P. Kumar, S. Mahapatra, P. Phukon, and T. Sarkar, *Phys. Rev. E* **86**, 051117 (2012), URL <https://link.aps.org/doi/10.1103/PhysRevE.86.051117>.
- [58] J. Cotler, N. Hunter-Jones, J. Liu, and B. Yoshida, *JHEP* **11**, 048 (2017), 1706.05400.
- [59] J. S. Cotler, G. Gur-Ari, M. Hanada, J. Polchinski, P. Saad, S. H. Shenker, D. Stanford, A. Streicher, and M. Tezuka, *JHEP* **05**, 118 (2017), [Erratum: *JHEP* 09, 002 (2018)], 1611.04650.
- [60] J. Liu, *Phys. Rev. D* **98**, 086026 (2018), 1806.05316.
- [61] G. Livan, M. Novaes, and P. Vivo, *Monograph Award* **63**, 914 (2018).
- [62] E. Brézin and A. Zee, *Phys. Rev. E* **49**, 2588 (1994), URL <https://link.aps.org/doi/10.1103/PhysRevE.49.2588>.
- [63] S. Schierenberg, F. Bruckmann, and T. Wettig, *Phys. Rev. E* **85**, 061130 (2012), URL <https://link.aps.org/doi/10.1103/PhysRevE.85.061130>.
- [64] T. H. Baker and P. J. Forrester, *Communications in Mathematical Physics* **188**, 175 (1997).
- [65] G. Le Caër, C. Male, and R. Delannay, *Physica A: Statistical Mechanics and its Applications* **383**, 190 (2007).
- [66] I. Dumitriu and A. Edelman, *Journal of Mathematical Physics* **47** (2006).
- [67] P. Desrosiers and P. J. Forrester, *Nuclear Physics B* **743**, 307 (2006).
- [68] P. J. Forrester, *Log-gases and random matrices (LMS-34)* (Princeton university press, 2010).
- [69] A. K. Das and A. Ghosh, *Physical Review E* **105**, 054121 (2022).
- [70] B. N. Parlett, *The symmetric eigenvalue problem* (SIAM, 1998).
- [71] P. Vivo and S. N. Majumdar, *Physica A: Statistical Mechanics and its Applications* **387**, 4839 (2008).
- [72] F. J. Dyson, *Journal of Mathematical Physics* **3**, 1191 (1962).
- [73] A. Nica and R. Speicher, *Lectures on the combinatorics of free probability*, vol. 13 (Cambridge University Press, 2006).
- [74] M. Bellitti, S. Morampudi, and C. R. Laumann, *Phys. Rev. B* **100**, 184201 (2019), 1908.02263.
- [75] H. A. Camargo, Y. Fu, V. Jahnke, K. Pal, and K.-Y. Kim, arXiv e-prints arXiv:2503.20338 (2025), 2503.20338.